

Electronic Supplementary Information for

**Amplified Circularly Polarized Phosphorescence from Co-Assemblies of Platinum(II) Complexes**

*Gyurim Park,<sup>a</sup> Hyungchae Kim,<sup>b</sup> Hoichang Yang,<sup>c</sup> Kyung Ryoul Park,<sup>b</sup> Inho Song,<sup>d,e</sup> Joon Hak Oh,<sup>d</sup> Changsoon Kim,<sup>b</sup> and Youngmin You<sup>a\*</sup>*

<sup>a</sup>Division of Chemical Engineering and Materials Science, Ewha Womans University, Seoul 03760, the Republic of Korea.

<sup>b</sup>Graduate School of Convergence Science and Technology and Inter-University Semiconductor Research Center, Seoul National University, Seoul 08826, the Republic of Korea.

<sup>c</sup>Department of Chemical Engineering, Inha University, Incheon 22212, the Republic of Korea.

<sup>d</sup>School of Chemical and Biological Engineering, Seoul National University, Seoul 08826, the Republic of Korea.

<sup>e</sup>Department of Chemical Engineering, Pohang University of Science and Technology (POSTECH), Pohang, Gyeongbuk 37673, the Republic of Korea.

\*To whom correspondence should be addressed: [odds2@ewha.ac.kr](mailto:odds2@ewha.ac.kr)

---

Experimental details	S3
<b>Table S1</b> Summary of $ g_{lum} $ and PLQY values reported previously for molecular CPL emitters	S9
<b>Table S2</b> Photophysical data for PtN, ( <i>R</i> )-PtBox and ( <i>S</i> )-PtBox	S20
<b>Table S3</b> Summary of the biexponential decay fit results of the photoluminescence traces shown in Fig. 5a	S21
<b>Fig. S1</b> Metal–metal-to-ligand charge-transfer (MMLCT) transition in PtN assemblies	S22
<b>Fig. S2</b> Quantum chemical predictions for torsional control of chiroptical properties	S23
<b>Fig. S3</b> <sup>1</sup> H NMR (300 MHz, CD <sub>2</sub> Cl <sub>2</sub> ) spectrum of PtN	S24
<b>Fig. S4</b> <sup>13</sup> C{ <sup>1</sup> H} NMR (126 MHz, CD <sub>2</sub> Cl <sub>2</sub> ) spectrum of PtN	S25
<b>Fig. S5</b> <sup>1</sup> H NMR (300 MHz, CD <sub>2</sub> Cl <sub>2</sub> ) spectrum of ( <i>R</i> )-PtBox	S26
<b>Fig. S6</b> <sup>13</sup> C{ <sup>1</sup> H} NMR (126 MHz, CD <sub>2</sub> Cl <sub>2</sub> ) spectrum of ( <i>R</i> )-PtBox	S27

<b>Fig. S7</b> <sup>1</sup> H NMR (300 MHz, CD <sub>2</sub> Cl <sub>2</sub> ) spectrum of (S)-PtBox	S28
<b>Fig. S8</b> <sup>13</sup> C{ <sup>1</sup> H} NMR (126 MHz, CD <sub>2</sub> Cl <sub>2</sub> ) spectrum of (S)-PtBox	S29
<b>Fig. S9</b> Supramolecular assembly formation of PtN	S30
<b>Fig. S10</b> Emergence of the metal–metal-to-ligand charge-transfer (MMLCT) transition during the self-assembly of PtN	S31
<b>Fig. S11</b> Minimal contribution of linear dichroism and birefringence	S32
<b>Fig. S12</b> Chiral amplification within the co-assemblies of PtBox/PtN	S33
<b>Fig. S13</b> Photophysical behaviors of (R)-PtBox and (S)-PtBox	S34
<b>Fig. S14</b> Metal–metal-to-ligand charge-transfer phosphorescence	S35
<b>Fig. S15</b> Spectral assignment	S36
<b>Fig. S16</b> Phosphorescence emission of PtN assemblies	S37
<b>Fig. S17</b> Intra-assembly energy transfer from PtBox to PtN	S38
<b>Fig. S18</b> Thermal disassembly of the self-assembled PtN	S39
<b>Fig. S19</b> Thermal disassembly of the co-assemblies of PtBox/PtN	S40
<b>Fig. S20</b> Circularly polarized phosphorescence from the co-assemblies of PtBox/PtN	S41
<b>References</b>	S42

**Quantum Chemical Calculations.** Geometry optimization was performed using Coulomb Attenuated Method-Becke's three-parameter (CAM-B3LYP) exchange-correlation functional, the "double- $\zeta$ " quality LANL2DZ basis set for the Pt atom, and the 6-311+G(d,p) basis set for all the other atoms. A pseudo potential (LANL2DZ) was applied to replace the inner core electrons of the Pt(II) atom, leaving the outer core [(5s)<sup>2</sup>(5p)<sup>6</sup>] electrons and the (5d)<sup>8</sup> valence electrons. Frequency calculations were subsequently performed to assess the stability of the convergence. For the rotatory strength calculations, geometry optimization was performed with fixing the dihedral angle of C–Pt...Pt–C using the modredundant keyword. Geometry optimization was performed for the initial geometries having the dihedral angles increased at a constant interval of 30°. Time-dependent density functional theory (TD–DFT) calculations were carried out for the optimized geometries using the same functional and basis sets. Twenty states were considered for the TD–DFT calculations. Geometry optimization and single-point calculations were performed using the Gaussian 09 program.<sup>1</sup>

**Materials and General Methods.** Commercially available chemicals were used as received unless otherwise stated. Potassium tetrachloroplatinate(II) (98.0%), 2-phenylpyridine(98.0%), 4,4'-bis(nonyl)-2,2'-bipyridine (97.0%), and 1,2-dichloroethane (>99.8%) were purchased from Sigma–Aldrich. (*R,R*)-2,2'-Isopropylidenebis(4-phenyl-2-oxazoline) (>96.0%), and (*S,S*)-2,2'-isopropylidenebis(4-phenyl-2-oxazoline) (>95.0%) were purchased from Tokyo Chemical Industry. <sup>1</sup>H and <sup>13</sup>C{<sup>1</sup>H} NMR spectra were collected with Bruker, Ultrashield 500 or 300 plus NMR spectrometers. Chemical shifts were referenced to (CH<sub>3</sub>)<sub>4</sub>Si. High resolution mass spectra (positive mode, FAB, *m*-NBA) were obtained by employing a JEOL, JMS-600W mass spectrometer. C, H, N, and O analyses were performed by employing Thermo Fisher Scientific, Flash1112 and Flash2000 elemental analyzers.

**Synthesis of [Pt<sub>2</sub>( $\mu$ -Cl)<sub>2</sub>(2-phenylpyridinate)<sub>2</sub>].** 2-Phenylpyridine (3.29 g, 21.2 mmol) and tetrachloropotassium platinate(II) (K<sub>2</sub>PtCl<sub>4</sub>) (4.00 g, 9.42 mmol) were dissolved in a mixture of 2-ethoxyethanol:water (3:1, v/v, total volume = 80 mL) in a 100 mL one-necked round-bottom flask equipped with a magnetic stir bar. The resulting mixture was stirred at 80 °C for 23 h under an Ar atmosphere. Yellow precipitates were formed upon cooling the solution to room temperature, which were filtered and washed thoroughly with water and ethyl ether. The crude product was dried *in vacuo*, and subjected to the next step without further purification.

**Synthesis of (R)-PtBox.** [Pt<sub>2</sub>(μ-Cl)<sub>2</sub>(2-phenylpyridinate)<sub>2</sub>] (0.45 g, 0.59 mmol) and (*R,R*)-2,2'-isopropylidenebis(4-phenyl-2-oxazoline) (0.39 g, 1.18 mmol) were dissolved in CH<sub>2</sub>Cl<sub>2</sub> (25 mL) in a 50 mL one-necked round-bottom flask equipped with a magnetic stir bar. AgClO<sub>4</sub> (0.250 g, 1.18 mmol) was added to a stirred solution under an Ar atmosphere. After stirring the solution for 4 h at room temperature, the reaction mixture was filtered through celite and concentrated under a reduced pressure. Addition of 150 mL ether into a 10 mL of the filtrate yielded pale yellow powder. The powder was collected by filtration. Silica gel column purification was performed with increasing the polarity of the eluent from CH<sub>2</sub>Cl<sub>2</sub>:CH<sub>3</sub>OH = 99:1 (v/v) to CH<sub>2</sub>Cl<sub>2</sub>:CH<sub>3</sub>OH = 19:1 (v/v). Finally, further purification employing preparatory TLC (Sigma–Aldrich) techniques was carried out with using CH<sub>2</sub>Cl<sub>2</sub>:CH<sub>3</sub>OH = 49:1 (v/v) as an eluent. Yellow powders were obtained in a 14% yield. *R<sub>f</sub>* = 0.34 (CH<sub>2</sub>Cl<sub>2</sub>:CH<sub>3</sub>OH = 19:1, v/v). <sup>1</sup>H NMR (300 MHz, CD<sub>2</sub>Cl<sub>2</sub>) δ (ppm): 1.84 (s, 3H), 2.57 (s, 3H), 4.76 (m, 1H), 4.87 (m, 1H), 4.98 (m, 1H), 5.09 (dd, *J* = 9.6, 4.5 Hz, 1H), 5.22 (t, *J* = 9.6 Hz, 1H), 5.85 (dd, *J* = 9.6, 4.5 Hz, 1H), 6.26 (m, 1H), 7.15 (m, 2H), 7.22 (m, 4H), 7.33 (m, 5H), 7.43 (m, 4H), 7.53 (dd, *J* = 8.4, 1.2 Hz, 1H), 7.62 (m, 1H). <sup>13</sup>C{<sup>1</sup>H} NMR (126 MHz, CD<sub>2</sub>Cl<sub>2</sub>) δ (ppm): 20.6, 26.1, 42.6, 70.5, 70.5, 77.7, 77.9, 119.1, 122.3, 124.2, 125.6, 127.4, 127.8, 129.2, 129.3, 129.5, 130.1, 130.2, 130.3, 130.3, 130.6, 133.7, 137.4, 137.6, 139.333 139.7, 140.7, 145.8, 151.7, 166.4, 175.5, 177.0. HR MS (FAB, *m*-NBA): Calcd for C<sub>32</sub>H<sub>30</sub>N<sub>3</sub>O<sub>2</sub>Pt ([M]<sup>+</sup>), 683.1986; found: 683.1990. Anal. calcd for C<sub>32</sub>H<sub>30</sub>ClN<sub>3</sub>O<sub>6</sub>Pt: C, 49.08; H, 3.86; N, 5.37; O, 12.26. Found: C, 48.80; H, 3.83; N, 5.30; O, 12.60.

**Synthesis of (S)-PtBox.** (*S*)-PtBox was prepared following the method identical to the synthesis of (*R*)-PtBox, except the use of (*S,S*)-2,2'-isopropylidenebis(4-phenyl-2-oxazoline) in place of (*R,R*)-2,2'-isopropylidenebis(4-phenyl-2-oxazoline). Yellow powders were obtained in a 23% yield. *R<sub>f</sub>* = 0.34 (CH<sub>2</sub>Cl<sub>2</sub>:CH<sub>3</sub>OH = 19:1, v/v). <sup>1</sup>H NMR (300 MHz, CD<sub>2</sub>Cl<sub>2</sub>) δ (ppm): 1.84 (s, 3H), 2.57 (s, 3H), 4.76 (m, 1H), 4.87 (m, 1H), 4.98 (m, 1H), 5.09 (dd, *J* = 9.6, 4.5 Hz, 1H), 5.22 (t, *J* = 9.6 Hz, 1H), 5.85 (dd, *J* = 9.6, 4.5 Hz, 1H), 6.26 (m, 1H), 7.15 (m, 2H), 7.22 (m, 4H), 7.33 (m, 5H), 7.43 (m, 4H), 7.53 (dd, *J* = 8.4, 1.2 Hz, 1H), 7.62 (m, 1H). <sup>13</sup>C{<sup>1</sup>H} NMR (126 MHz, CD<sub>2</sub>Cl<sub>2</sub>) δ (ppm): 20.5, 26.1, 42.5, 70.5, 70.5, 77.7, 77.9, 119.1, 122.2, 124.2, 125.6, 127.4, 127.8, 129.2, 129.3, 129.5, 130.1, 130.2, 130.3, 130.3, 130.6, 133.7, 137.4, 137.6, 139.4, 139.7, 140.7, 145.8, 151.7, 166.4, 175.4, 177.0. HR MS (FAB, *m*-NBA): Calcd for C<sub>32</sub>H<sub>30</sub>N<sub>3</sub>O<sub>2</sub>Pt ([M]<sup>+</sup>), 683.1986; found: 683.1993. Anal. calcd for C<sub>32</sub>H<sub>30</sub>ClN<sub>3</sub>O<sub>6</sub>Pt: C, 49.08; H, 3.86; N, 5.37; O, 12.26. Found: C, 49.31; H, 3.91; N, 5.37; O, 12.19.

**Synthesis of PtN.** PtN was prepared following the method identical to the synthesis of (*R*)-PtBox, except the use of 4,4'-bis(nonyl)-2,2'-bipyridine (0.32 g, 0.78 mmol) in place of (*R,R*)-2,2'-

isopropylidenebis(4-phenyl-2-oxazoline). Yellow powders were obtained in a 69% yield.  $R_f = 0.42$  (CH<sub>2</sub>Cl<sub>2</sub>:CH<sub>3</sub>OH = 19:1, v/v). <sup>1</sup>H NMR (300 MHz, CD<sub>2</sub>Cl<sub>2</sub>)  $\delta$  (ppm): 0.88 (m, 5H), 1.35 (m, 19H), 1.79 (m, 4H), 2.88 (m, 4H), 7.29 (m, 3H), 7.50 (m, 2H), 7.62 (d,  $J = 7.2$  Hz, 1H), 7.74 (dd,  $J = 5.7, 1.2$  Hz, 1H), 7.86 (d,  $J = 7.8$  Hz, 1H), 8.05 (t,  $J = 7.5$  Hz, 1H), 8.10 (s, 1H), 8.15 (s, 1H), 8.76 (d,  $J = 6.0$  Hz, 1H), 8.85 (d,  $J = 6.0$  Hz, 1H), 9.21 (d,  $J = 5.7$  Hz, 1H). <sup>13</sup>C{<sup>1</sup>H} NMR (126 MHz, CD<sub>2</sub>Cl<sub>2</sub>)  $\delta$  (ppm): 14.5, 23.2, 29.9, 30.0, 30.1, 30.4, 30.6, 32.5, 36.1, 36.1, 120.2, 124.0, 124.4, 124.4, 124.5, 125.4, 127.9, 128.3, 130.6, 132.9, 140.3, 141.3, 145.6, 148.8, 149.9, 152.0, 154.8, 156.7, 157.6, 157.9, 167.0. HR MS (FAB, *m*-NBA): Calcd for C<sub>39</sub>H<sub>52</sub>N<sub>3</sub>Pt ([M]<sup>+</sup>), 757.3809; found: 757.3821.

**Steady-State UV-vis Absorption Measurements.** UV-vis absorption spectra were collected on an Agilent, Cary 300 spectrophotometer at 298 K. Sample solutions were prepared prior to measurements at concentrations of 10 or 50  $\mu$ M in THF, unless otherwise stated. The solution was delivered into a quartz cell (Hellma, beam path length = 1.0 cm). PtBox/PtN co-assemblies were prepared by dissolving 2.0 mg PtBox and 5.0 mg PtN in 245 mg 1,2-dichloroethane (i.e., 2.0 wt % total solute; PtBox:PtN = 2:5, w/w). The mixture solution was dropcast onto a 2.0 cm  $\times$  2.0 cm quartz plate, and dried slowly under an atmospheric pressure at 298 K. Self-assemblies of PtN were prepared similarly.

**Steady-State Electronic Circular Dichroism Measurements.** Electronic circular dichroism (ECD) spectra were collected on a Jasco, J-1500 spectropolarimeter at 298 K. Sample solutions were prepared prior to measurements at concentrations of 50  $\mu$ M or 1.0 mM in THF. A quartz cell (Hellma, beam path length = 1.0 cm) was employed. PtBox/PtN co-assemblies were prepared by dissolving 2.0 mg PtBox and 5.0 mg PtN in 245 mg 1,2-dichloroethane (i.e., 2.0 wt % total solute; PtBox:PtN = 2:5, w/w). The mixture solution was dropcast onto a 2.0 cm  $\times$  2.0 cm quartz plate, and dried slowly under atmospheric pressure at 298 K. Self-assemblies of PtN were prepared similarly. Measurement conditions: scan rate, 500 nm min<sup>-1</sup>; detection range, 280–800 nm.

**Atomic Force Microscopy.** Co-assembly films were prepared by drop-casting 1,2-dichloroethane solution (245 mg) containing 5.0 mg PtN and 2.0 mg PtBox onto a 1 cm  $\times$  1 cm quartz plate. PtN self-assembly films were obtained from a 1,2-dichloroethane solution (245 mg) containing 5.0 mg PtN. The drop-cast films were dried thoroughly prior to measurements. Morphologies of the assembly films were characterized with employing a Bruker, Multimode 8 atomic force microscope.

**Confocal Laser Scanning Microscopy.** Assembly films were prepared following the method identical for the AFM measurements. Morphologies of the PtN self-assemblies and the PtBox/PtN co-assemblies were visualized by recording their phosphorescence images. The phosphorescence images were acquired with employing a Carl Zeiss, LSM 510 META confocal laser scanning

microscope. An excitation beam (405 nm) was focused onto the film, and the phosphorescence signals were acquired through the emission range 470–700 nm. Phosphorescence images and mean intensities were analyzed using a Carl Zeiss, LSM 510 version 4.0 software.

**Field-Emission Scanning Electron Microscopy.** Assembly films were prepared following the method identical for the AFM measurements. The films were additionally deposited with thin platinum using a Hitachi, MC1000 Ion sputter coater at 15 mA for 60 s. The surface of the assemblies were visualized employing a Hitachi, SU8220 field-emission scanning electron microscope.

**Grazing Incident X-Ray Diffraction Experiments.** Synchrotron-based 2D grazing incident X-ray diffraction (2D GIXD) experiments were performed for the dropcast films at beamline 6D of Pohang Acceleration Laboratory (PAL), Korea. With regard to the GIXD mode, a sample was mounted onto a three-axis goniometer and the intensity of scattered X-ray was recorded with a 2D detector. The incident angle of the X-ray beam in the sample was remained below  $0.18^\circ$ .

**Steady-State Phosphorescence Measurements.** Phosphorescence spectra were obtained using a Photon Technology International, Quanta Master 400 scanning spectrofluorometer at 298 K. The solutions (THF) and co-assemblies (quartz plates) used for the steady-state UV–vis absorption studies were employed for the phosphorescence measurements. The solutions were deaerated by bubbling Ar prior to the measurements. A quartz cell (Hellma, beam path length = 1.0 cm) was employed for solution samples. The co-assemblies on quartz plates were placed on a solid sample stage (Photon Technology International), and angles were adjusted to keep an incident excitation beam to be  $45^\circ$  to the vertical axis of the sample. The excitation wavelengths were 370 nm and 326 nm for PtN and PtBox, respectively. The phosphorescence spectra were recorded in the emission range 400–700 nm.

**Determination of Photoluminescence Lifetimes.** Deaerated THF solutions of 50  $\mu\text{M}$  (*R*)-PtBox, (*S*)-PtBox, and PtN were employed. Co-assemblies of (*R*)-PtBox/PtN or (*S*)-PtBox/PtN and self-assemblies of PtN were freshly prepared by dropcasting 1,2-dichloroethane solutions (2.0 wt % total solute; PtBox:PtN = 1–20:100, w/w) onto 2.0 cm  $\times$  2.0 cm quartz plates, prior to measurements. Photoluminescence decay traces were acquired based on time-correlated single-photon-counting (TCSPC) techniques, using a PicoQuant, FluoTime 200 instrument after nanosecond pulsed laser excitation at 377 nm (pulse duration = 1.6 ns). Transient photon signals were collected at  $\lambda_{\text{obs}} = 480$  nm, 520 nm, or 615 nm through an automated motorized monochromator. The photon acquisition was terminated when the accumulated photon count reached  $10^4$ . Photoluminescence decay traces were analyzed using mono- or biexponential decay models embedded in an OriginLab, OriginPro

2018 software. In the case of biphasic decay, an average photoluminescence lifetime ( $\tau_{\text{obs}}$ ) values were calculated from the relationship  $\tau_{\text{obs}} = \sum A_i \tau_i^2 / \sum A_i \tau_i$  ( $i = 1-2$ ), where  $A_i$  and  $\tau_i$  are the pre-exponential factor and the time constant, respectively.

**Determination of Relative Photoluminescence Quantum Yields.** The relative photoluminescence quantum yield (PLQY) was determined for the solutions, following the equation  $\text{PLQY} = \text{PLQY}_{\text{ref}} \times (I/I_{\text{ref}}) \times (A_{\text{ref}}/A) \times (n/n_{\text{ref}})^2$ , where  $A$ ,  $I$ , and  $n$  are absorbance at the excitation wavelength, the integrated photoluminescence intensity, and the refractive index of the solvent, respectively. 9,10-diphenylanthracene ( $\text{PLQY}_{\text{ref}} = 1.00$ , toluene;  $\lambda_{\text{ex}} = 366$  nm) was used as the reference material (ref).<sup>2</sup> 10  $\mu\text{M}$  samples or the reference were dissolved in toluene (spectrophotometric grade) which were thoroughly deaerated prior to the measurements. Photoluminescence spectra were collected at 298 K in the emission range 400–700 nm. The spectra were integrated with employing an OriginLab, OriginPro 2018 software.

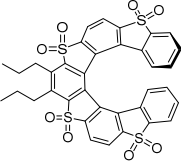
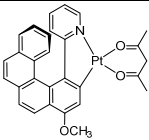
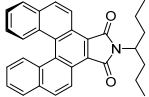
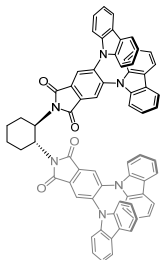
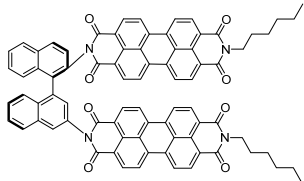
**Determination of Absolute Photoluminescence Quantum Yields.** The photoluminescence quantum yields of the co-assemblies of (*R*)-PtBox/PtN or (*S*)-PtBox/PtN and the self-assemblies of PtN were determined absolutely. The assemblies were prepared onto 2.0 cm  $\times$  2.0 cm quartz plates prior to the measurement. Photon flux of an excitation beam (400 nm;  $I_{\text{ex}}(0)$ ) was quantified in the absence of a sample. The sample was placed into an integrating sphere (Photon Technology International), and an excitation beam was focused at the center of the sample. The flux of the excitation photons ( $I_{\text{ex}}(s)$ ) was quantitated. Finally, photon flux of the photoluminescence emission from the sample ( $I_{\text{em}}$ ) was measured with employing the following conditions: integration time, 0.1 s; step size, 0.0625 nm; emission range, 400–800 nm. Note that all the measurements were performed without performing deaeration. A ratio of the absorbed photon flux and the emission photon flux corresponded to the PLQY:  $\text{PLQY} = I_{\text{em}} / (I_{\text{ex}}(0) - I_{\text{ex}}(s))$ . The measurement was repeated in triplicate for each fresh sample.

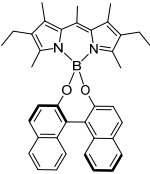
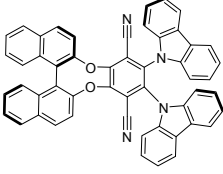
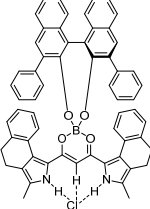
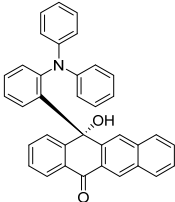
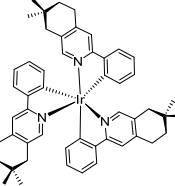
**Circularly Polarized Luminescence Measurements.** Circularly polarized luminescence (CPL) measurements were performed using a Thorlabs, M365LP1 light emitting diode as a photoexcitation source. The emitted photons were collected by an Andor, iDUS DU401 charge-coupled device after passing through a circular analyzer consisting of a Thorlabs, AQWP05M-600 achromatic quarter-wave retardation plate, a Thorlabs, LPVISE100-A linear polarizer, and a Shamrock, SR303i spectrometer. To detect the left- or right-circularly polarized light, the crystal axis of the retarder was manipulated to be oriented at  $+45^\circ$  or  $-45^\circ$  with respect to that of the linear polarizer using a computer-controlled motorized stage. We found that our spectroscopic system is working properly by successfully reproducing the CPL dissymmetry spectrum of 5.5 mM europium

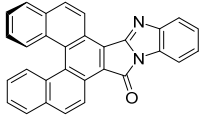
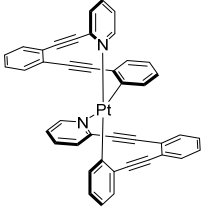
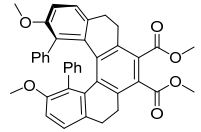
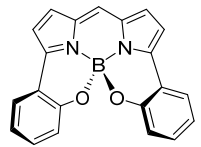
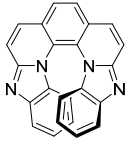
tris[3-(trifluoromethylhydroxymethylene)-(+)-camphorate] ([Eu(facam)<sub>3</sub>]) diluted in DMSO, which is widely used as a standard.<sup>3</sup>

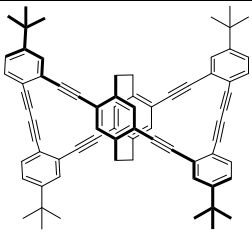
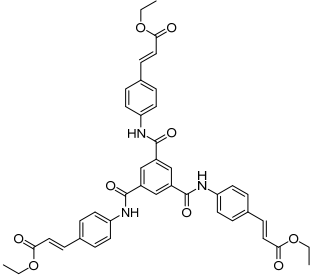
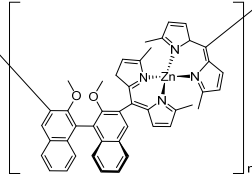
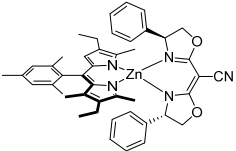
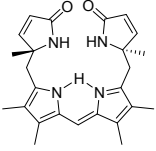


**Table S1.** Summary of  $|g_{lum}|$  and PLQY Values Reported Previously for Molecular CPL Emitters

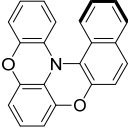
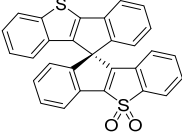
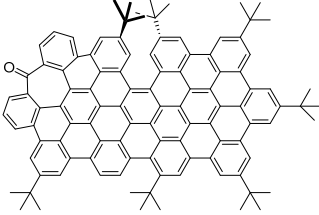
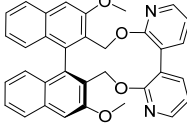
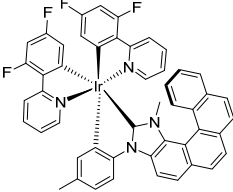
entry	structure (condition)	$ g_{lum} $	PLQY	reference
1	 (THF solution)	0.00083	0.27	4
2	 (1.0 mM in degassed CH <sub>2</sub> Cl <sub>2</sub> )	0.013	0.10	5
3	 (THF solution)	0.0024	0.37	6
4	 (neat film)	0.0011	0.98	7
5	 (toluene solution)	0.0030	0.88	8

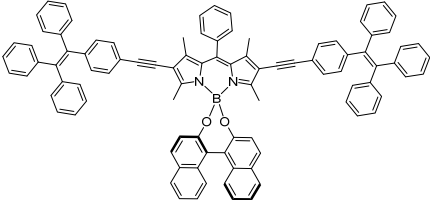
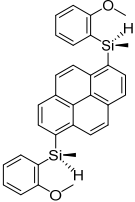
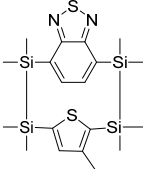
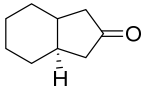
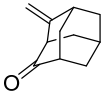
6		0.0010	0.44	9
(1.0 mM in degassed $\text{CHCl}_3$ )				
7		0.0013	0.53	10
(1.0 mM in degassed toluene)				
8		0.0020	0.51	11
(10 $\mu\text{M}$ in $\text{CH}_2\text{Cl}_2$ )				
9		0.0011	0.26	12
(88 $\mu\text{M}$ in toluene)				
10		0.0032	0.64	13
(CH <sub>3</sub> CN solution)				

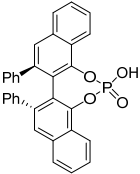
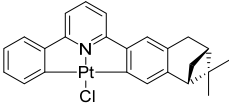
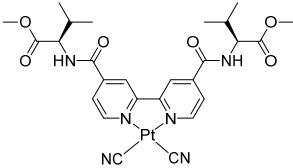
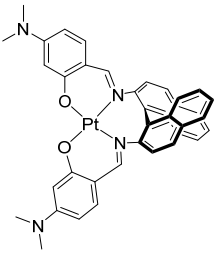
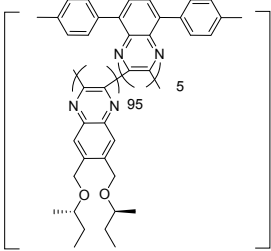
11		0.0095	0.06	14
	(20 $\mu$ M in $\text{CH}_2\text{Cl}_2$ )			
12		0.0010	0.07	15
	( $\text{CH}_2\text{Cl}_2$ solution)			
13		0.0066	0.03	16
	(50 $\mu$ M in THF)			
14		0.0047	0.65	17
	( $\text{CH}_3\text{CN}$ solution)			
15		0.0090	0.39	18
	(10 $\mu$ M in $\text{CH}_2\text{Cl}_2$ )			

16	 <p>(10 <math>\mu</math>M in <math>\text{CHCl}_3</math>)</p>	0.011	0.45	19
17	 <p>(suspension in DMF:water = 5:2, v/v)</p>	0.0080	0.11	20
18	 <p>(toluene solution)</p>	0.0026	0.01	21
19	 <p>(<math>\text{CH}_2\text{Cl}_2</math> solution)</p>	0.0010	0.59	22
20	 <p>(<math>\text{CH}_2\text{Cl}_2</math> solution)</p>	0.00094	0.48	23

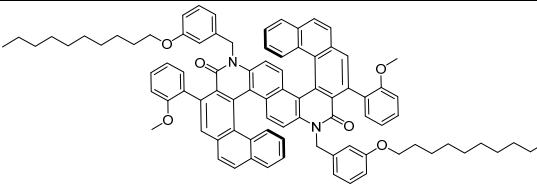
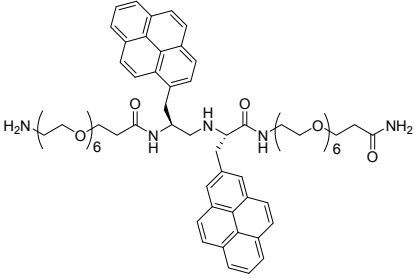
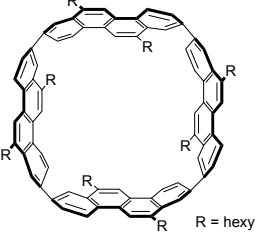
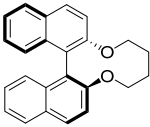
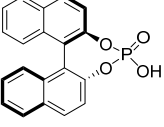
21		0.010	0.32	24
<p>(200 <math>\mu\text{M}</math> suspension in <math>\text{CH}_2\text{Cl}_2</math>:hexane = 1:9, v/v)</p>				
22		0.079	0.11	25
<p>(5 <math>\mu\text{M}</math> suspension in <math>\text{CH}_3\text{OH}</math>:water = 1:1, v/v)</p>				
23		0.010	0.09	26
<p>(5 <math>\mu\text{M}</math> suspension in <math>\text{CH}_3\text{OH}</math>:water = 1:1, v/v)</p>				
24		0.0011	0.26	27
<p>(100 <math>\mu\text{M}</math> in <math>\text{CHCl}_3</math>)</p>				
25		0.0050	0.42	28
<p>(neat film)</p>				

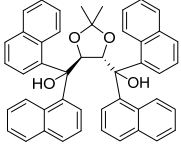
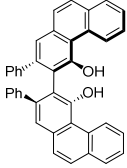
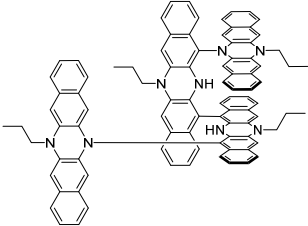
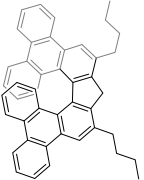
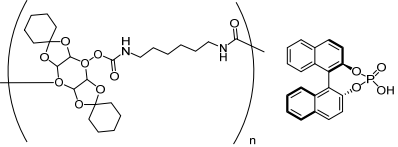
26		0.0047	0.86	29
	(CH <sub>2</sub> Cl <sub>2</sub> solution)			
27		0.0030	0.01	30
	(CH <sub>2</sub> Cl <sub>2</sub> solution)			
28		0.00023	0.13	31
	(10 μM in CH <sub>2</sub> Cl <sub>2</sub> )			
29		0.0016	0.15	32
	(10 μM in CH <sub>2</sub> Cl <sub>2</sub> )			
30		0.0037	0.09	33
	(10 μM in CH <sub>2</sub> Cl <sub>2</sub> )			

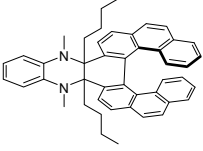
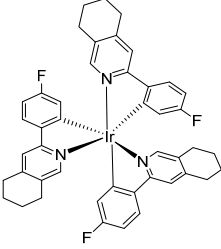
31		0.0020	0.58	34
<p>(10 <math>\mu</math>M suspension in <math>\text{CH}_2\text{Cl}_2</math>:hexane = 1:9, v/v)</p>				
32		0.0080	0.42	35
<p>(4.0 mM in <math>\text{CH}_2\text{Cl}_2</math>)</p>				
33		0.0017	0.05	36
<p>(15 <math>\mu</math>M in cyclohexane)</p>				
34		0.035	0.001	37
<p>(50 mM in isooctane)</p>				
35		0.0063	0.02	38
<p>(5.0 mM in heptane)</p>				

36		0.0035	0.12	39
	(100 $\mu$ M in $\text{CHCl}_3$ )			
37		0.00010	0.66	40
	(1.0 mM in $\text{CH}_3\text{CN}$ )			
38		0.040	0.03	41
	$(\text{CH}_2\text{Cl}_2, -88^\circ\text{C})$			
39		0.0050	0.05	42
	(5 wt % in PVK film)			
40		0.0011	0.04	43
	$(1.83 \times 10^{-2} \text{ g L}^{-1}$ in $\text{CHCl}_3$ )			



41		0.028	0.19	44
(10 $\mu$ M in $\text{CHCl}_3$ )				
42		0.0072	0.09	45
(100 $\mu$ M in $\text{CHCl}_3$ )				
43	 <p data-bbox="676 1305 735 1323">R = hexyl</p>	0.15	0.80	46
(toluene solution)				
44		0.0014	0.25	47
(1.0 mM in $\text{CHCl}_3$ )				
45		0.0015	0.29	48
( $\text{CHCl}_3$ solution)				

46		0.0013	0.20	49
	(1.0 mM in CHCl <sub>3</sub> )			
47		0.0094	0.02	50
	(10 μM in CHCl <sub>3</sub> )			
48		0.0025	0.47	51
	(3.0 μM in CH <sub>2</sub> Cl <sub>2</sub> )			
49		0.032	0.30	52
	(20 μM in CHCl <sub>3</sub> )			
50		0.0015	0.26	53
	(composite film)			

51		0.004	0.25	54
	(THF solution)			
52		0.002	0.34	55
	(25 $\mu$ M in toluene)			

**Table S2.** Photophysical Data for PtN, (*R*)-PtBox and (*S*)-PtBox

	$\lambda_{\text{abs}}$ (nm) <sup>a</sup>	$\epsilon$ at $\lambda_{\text{abs}}$ (10 <sup>3</sup> M <sup>-1</sup> cm <sup>-1</sup> ) <sup>b</sup>	$\lambda_{\text{em}}$ (nm) <sup>c</sup>	PLQY <sup>d</sup>	$\tau_{\text{obs}}$ ( $\mu$ s) <sup>e</sup>	$k_r$ (10 <sup>4</sup> s <sup>-1</sup> ) <sup>f</sup>	$k_{\text{nr}}$ (10 <sup>6</sup> s <sup>-1</sup> ) <sup>g</sup>	$g_{\text{abs}}$ <sup>h</sup>	$g_{\text{lum}}$ <sup>i</sup>
PtN	430 <sup>j</sup>	1.5 <sup>j</sup>	480 <sup>j</sup>	0.001 <sup>j</sup>	1.2 <sup>j</sup>	0.083 <sup>j</sup>	0.83 <sup>j</sup>	N.A	N.A
	490 <sup>k</sup>	N.A. <sup>k</sup>	615 <sup>k</sup>	0.006 <sup>k,l</sup>	0.61 <sup>k</sup>	0.98 <sup>k</sup>	1.62 <sup>k</sup>		
( <i>R</i> )- PtBox	380 <sup>j</sup>	2.0 <sup>j</sup>	520 <sup>j</sup>	0.02 <sup>j</sup>	3.4 <sup>j</sup>	0.59 <sup>j</sup>	2.9 <sup>j</sup>	+3.7 ×	N.A. <sup>j</sup>
	380 <sup>k</sup>	N.A. <sup>k</sup>	520 <sup>k</sup>	0.008 <sup>k,l</sup>	0.52 <sup>k</sup>	1.5 <sup>k</sup>	1.9 <sup>k</sup>	10 <sup>-5 m</sup>	<0.001 <sup>k</sup>
( <i>S</i> )- PtBox	380 <sup>j</sup>	2.0 <sup>j</sup>	520 <sup>j</sup>	0.02 <sup>j</sup>	3.7 <sup>j</sup>	0.54 <sup>j</sup>	2.6 <sup>j</sup>	-4.3 ×	N.A. <sup>j</sup>
	380 <sup>k</sup>	N.A. <sup>k</sup>	520 <sup>k</sup>	0.006 <sup>k,l</sup>	0.44 <sup>k</sup>	1.4 <sup>k</sup>	2.2 <sup>k</sup>	10 <sup>-5 m</sup>	<0.001 <sup>k</sup>

<sup>a</sup>Absorption peak wavelength. <sup>b</sup>Molar absorbance at the peak wavelength. <sup>c</sup>Photoluminescence peak wavelength. Excitation wavelengths = 370 nm (PtN) and 326 nm ((*R*)- and (*S*)-PtBox). <sup>d</sup>Photoluminescence quantum yields determined relatively to that of 9,10-diphenylanthracene (PLQY = 1.00). <sup>e</sup>Photoluminescence lifetime obtained after pulsed laser excitation at 377 nm (temporal resolution = 1.6 ns; observation wavelength ( $\lambda_{\text{obs}}$ ) = 480 nm (PtN solution), 615 nm (PtN film), and 520 nm ((*R*)- and (*S*)-PtBox)). <sup>f</sup>Radiative rate constant,  $k_r = \text{PLQY}/\tau_{\text{obs}}$ . <sup>g</sup>Non-radiative rate constant,  $k_{\text{nr}} = (1 - \text{PLQY})/\tau_{\text{obs}}$ . <sup>h</sup>Absorption dissymmetry factor. <sup>i</sup>Luminescence dissymmetry factor. <sup>j</sup>10  $\mu$ M in deaerated toluene. <sup>k</sup>Dropcast film on a quartz plate. <sup>l</sup>Absolute PLQY. <sup>m</sup>1.0 mM in THF.  $\lambda_{\text{obs}} = 308$  nm.

**Table S3.** Summary of the Biexponential Decay Fit Results of the Photoluminescence Traces Shown in Fig. 5a<sup>a</sup>

	$A_1$	$\tau_1$ ( $\mu$ s)	$A_2$	$\tau_2$ ( $\mu$ s)	$\tau_{\text{avg}}$ ( $\mu$ s) <sup>b</sup>
(R)-PtBox	43	0.29	52	3.6	3.4
(R)-PtBox/PtN co-assemblies	107	0.021	1696	0.0014	0.011
(S)-PtBox	46	0.23	55	3.9	3.7
(S)-PtBox/PtN co-assemblies	128	0.020	1382	0.0017	0.011

<sup>a</sup> $\lambda_{\text{obs}} = 520$  nm. Photoluminescence intensity =  $A_1\exp(-t/\tau_1) + A_2\exp(-t/\tau_2) + A_0$ .  $\tau_{\text{avg}} = (\sum A_i \tau_i^2) / (\sum A_i \tau_i)$  ( $i = 1-2$ ).

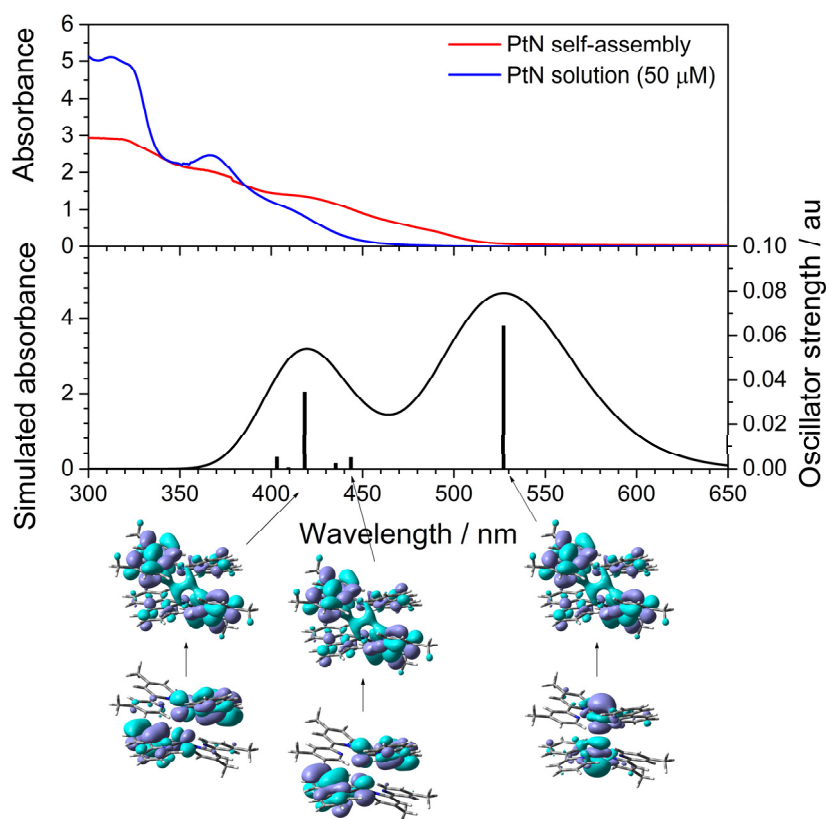


**Fig. S1** Metal–metal-to-ligand charge-transfer (MMLCT) transition in PtN assemblies. Comparison of the experimental (top: red, dropcast film; blue, 50  $\mu\text{M}$  solution in 1,4-dioxane; absorbance of the solution spectrum is multiplied by a factor of eight) and the calculated (bottom; TD-CAM-B3LYP/LANL2DZ:6-311+G(d,p)//CAM-B3LYP/LANL2DZ:6-311+G(d,p)) UV-vis absorption spectra of PtN. Shown below are isosurface (isovalue = 0.0200) of the molecular orbitals that participate in the electronic transitions at 527 nm, 443 nm and 418 nm (from the right). Note that the electronic transition at 527 nm involves MMLCT character of  $d_z^2\sigma^* \rightarrow \pi^*$ . The underestimation of the MMLCT transition energy may be due to the use of the B3LYP functional.

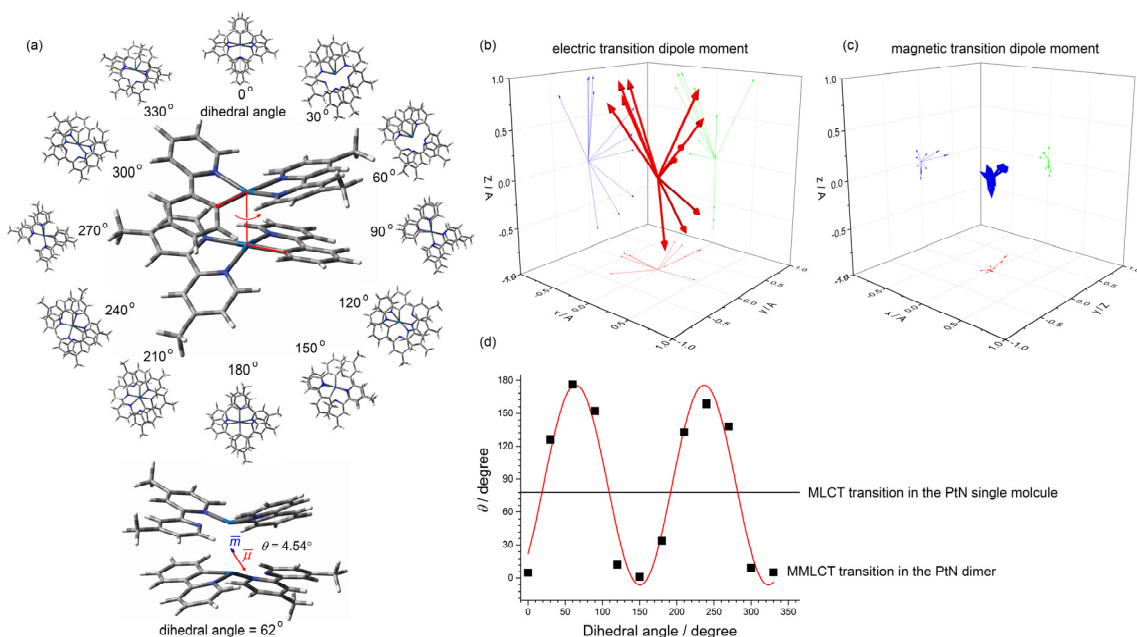


**Fig. S2** Quantum chemical predictions for torsional control of chiroptical properties. Quantum chemical calculations of the chiroptical properties of a pair of a truncated form of PtN (PtN dimer) obtained with varying the dihedral angle of C–Pt...Pt–C (the red arrow in the structure). (a) Optimized geometries of the PtN dimers at fixed dihedral angles. The dihedral angles were increased from 0° to 330° at 30° intervals. The bottom structure is the fully optimized geometry of a PtN dimer obtained without the dihedral constraint. The blue and red arrows denote the electric and the magnetic transition dipole moments, respectively. The angle between the two transition dipole moment ( $\theta$ ) is 4.54°. (b) Electric transition dipole moments ( $\mu$ ) of the metal–metal-to-ligand charge-transfer (MMLCT) transition in the PtN dimers calculated with varying the dihedral angle. (c) Magnetic transition dipole moments ( $m$ ) of the MMLCT transition in the PtN dimers calculated with varying the dihedral angle. (d) Corresponding angles ( $\theta$ , black squares) between  $\mu$  and  $m$ . The  $\theta$  values were calculated from the equation  $\theta = \cos^{-1} \{ (m \cdot \mu) / (|m||\mu|) \}$ . The red oscillatory curve is a visual guide for the change in  $\theta$ . The horizontal line at  $y = 79.2^\circ$  indicates the  $\theta$  of the metal-to-ligand charge-transfer (MLCT) transition in the PtN singlet molecule. c.f., (*R*)-PtBox,  $\theta = 85.26^\circ$ ; (*S*)-PtBox,  $\theta = 85.55^\circ$ . Calculation conditions: TD–CAM-B3LYP/LANL2DZ:6–311+G(d,p)//CAM-B3LYP/LANL2DZ:6–311+G(d,p). Twenty states were considered for the TD–DFT calculations.





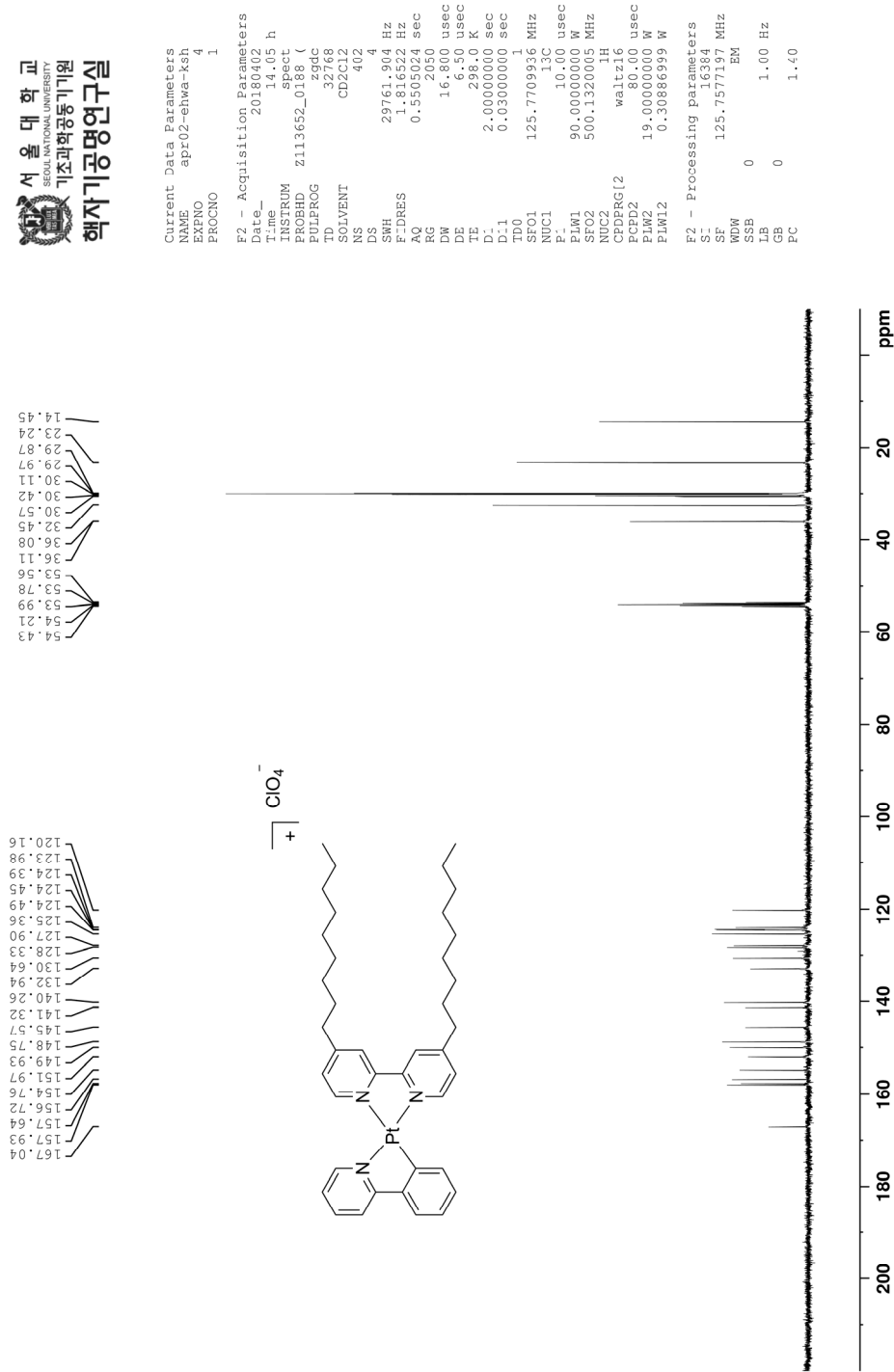


Fig. S4  $^{13}\text{C}\{^1\text{H}\}$  NMR (126 MHz,  $\text{CD}_2\text{Cl}_2$ ) spectrum of PtN.

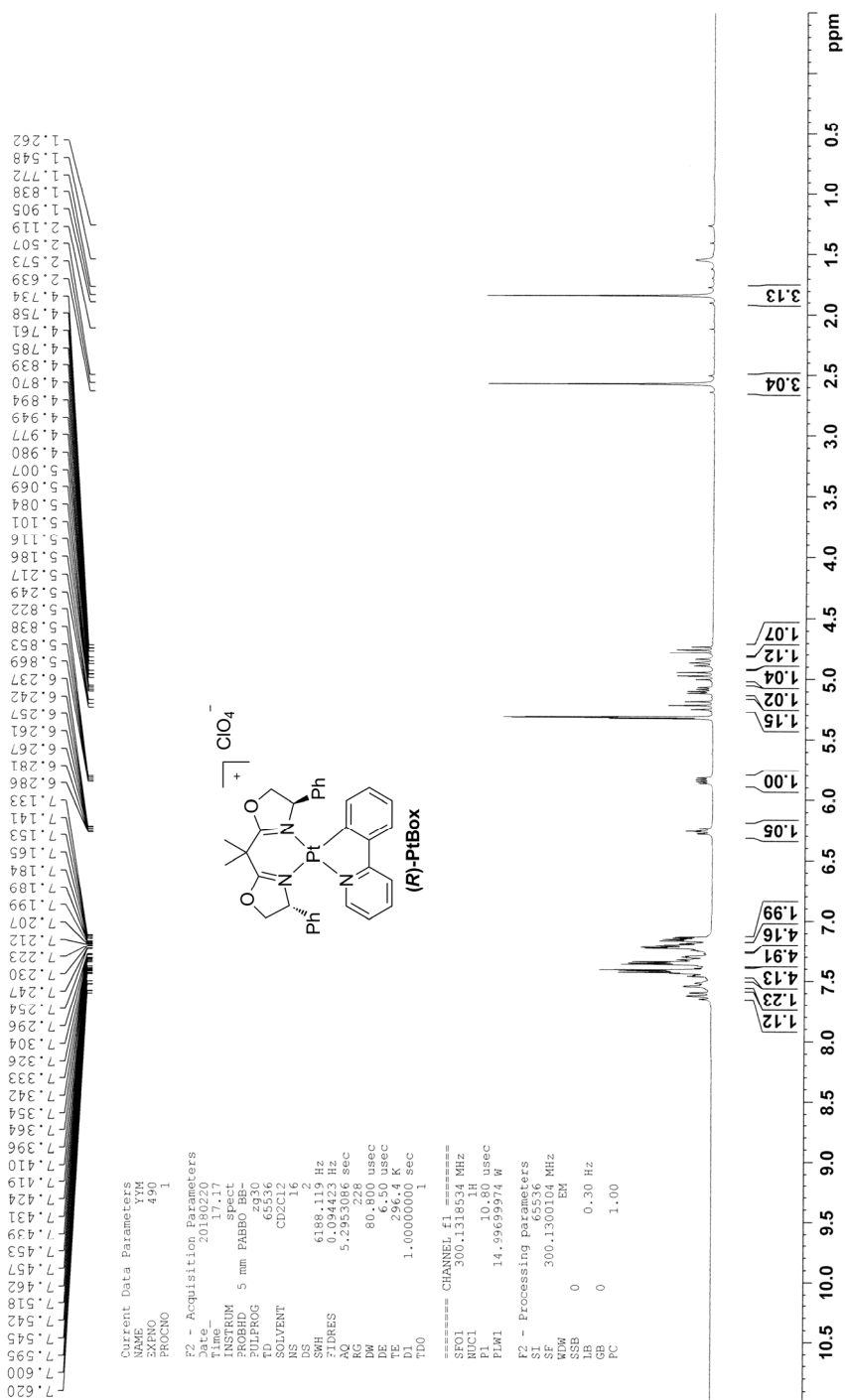


Fig. S5 <sup>1</sup>H NMR (300 MHz, CD<sub>2</sub>Cl<sub>2</sub>) spectrum of (R)-PtBox.

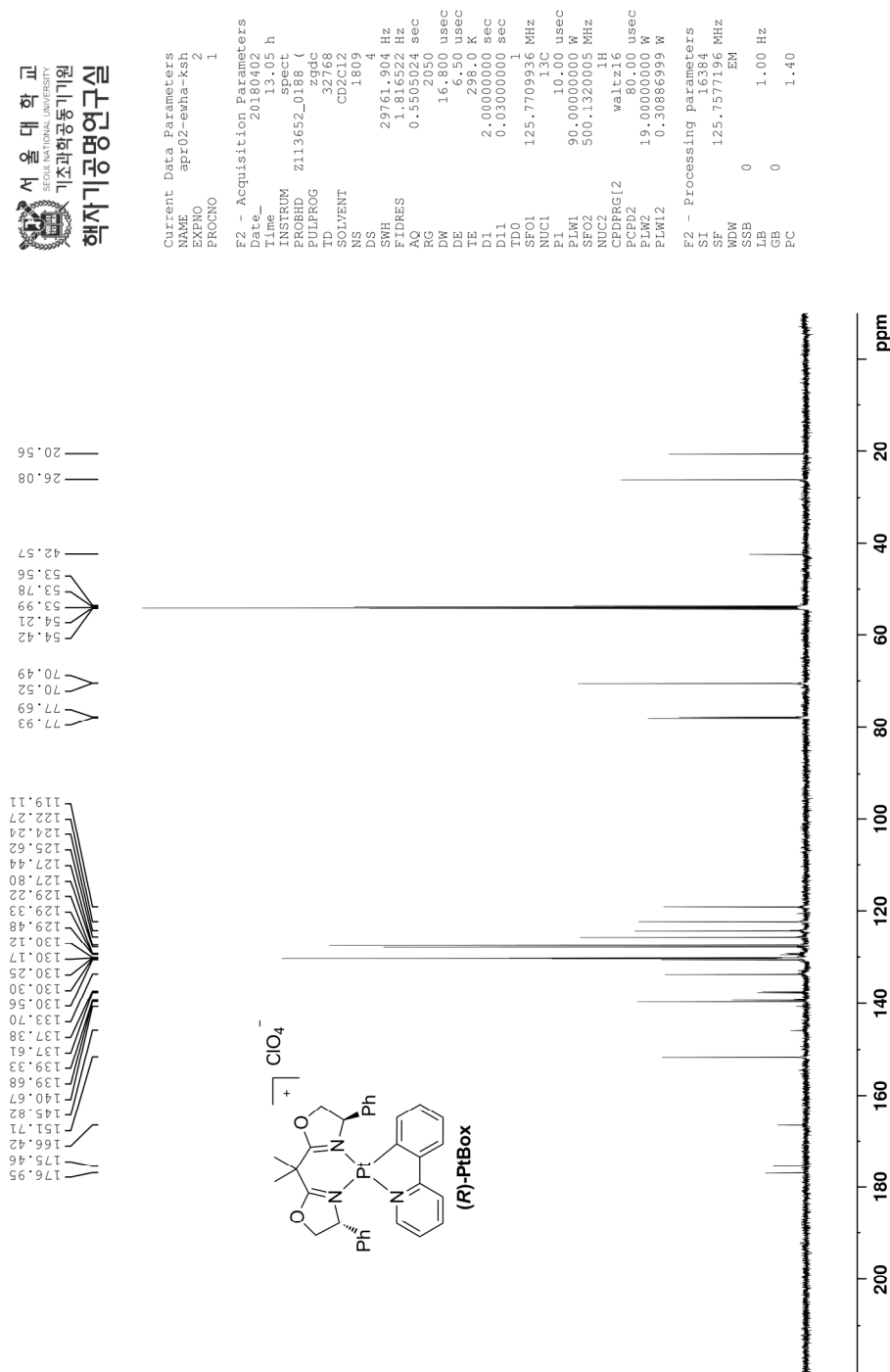


Fig. S6  $^{13}\text{C}\{^1\text{H}\}$  NMR (126 MHz,  $\text{CD}_2\text{Cl}_2$ ) spectrum of (R)-PtBox.

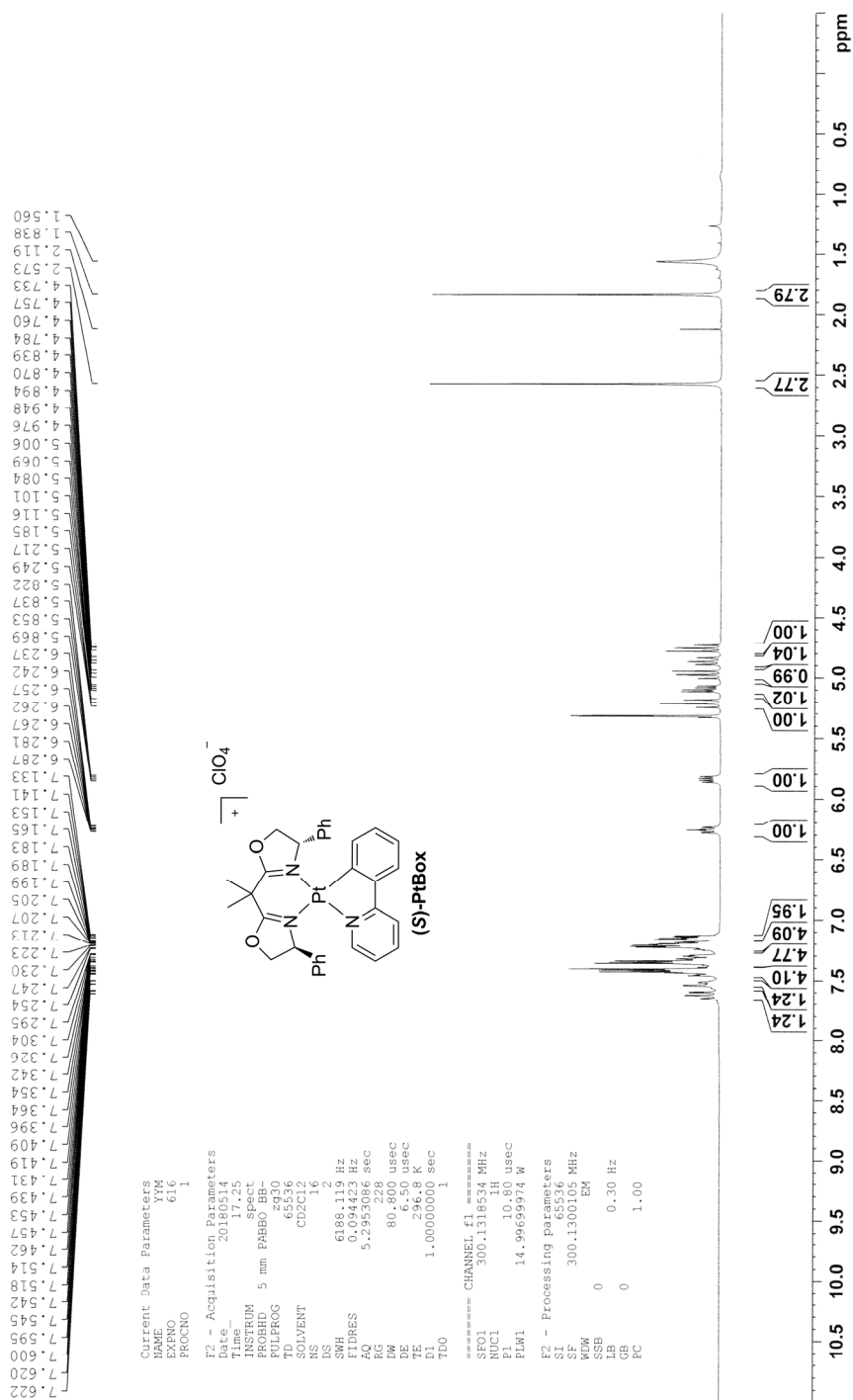


Fig. S7 <sup>1</sup>H NMR (300 MHz, CD<sub>2</sub>Cl<sub>2</sub>) spectrum of (S)-PtBox.

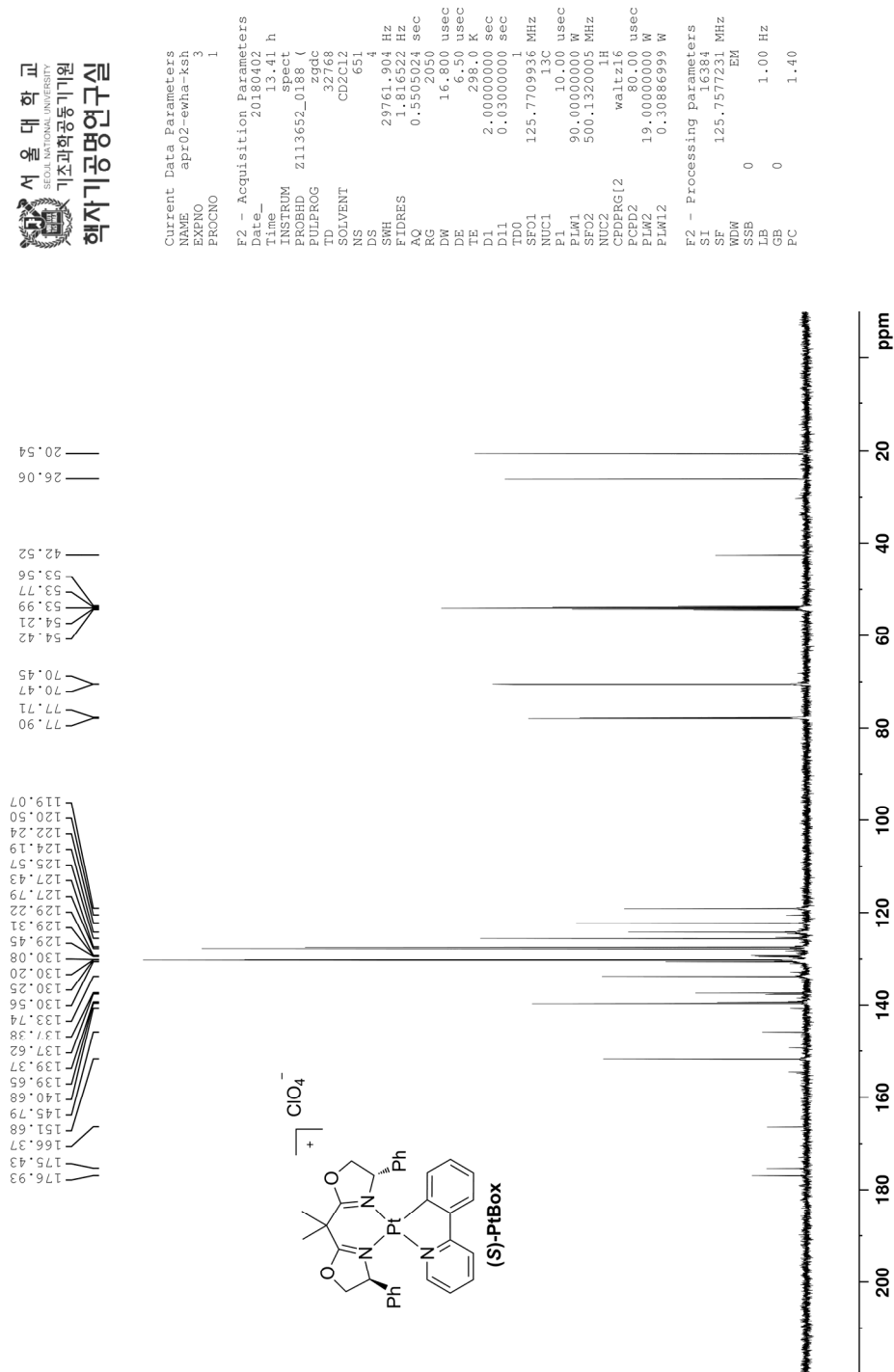
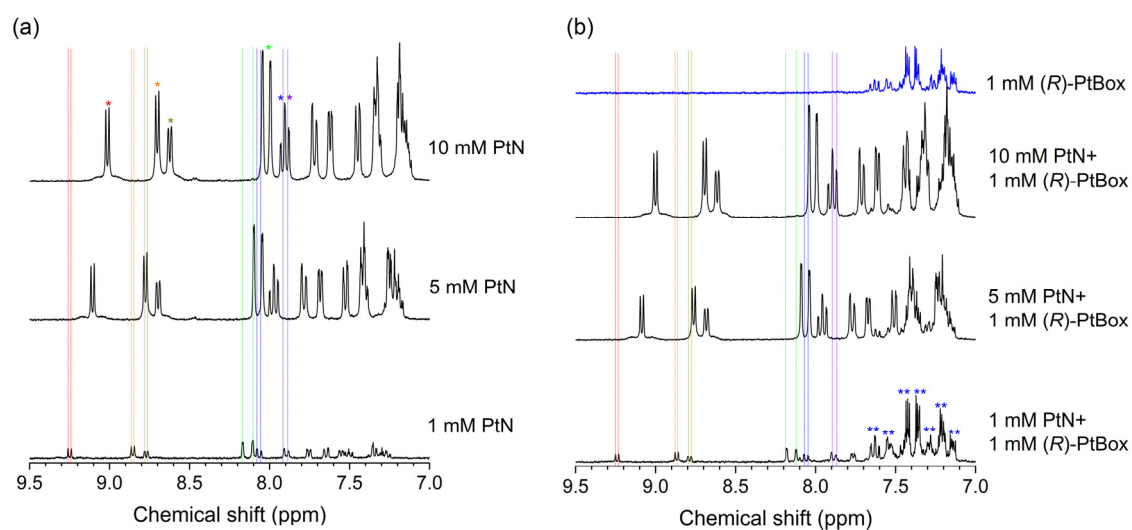
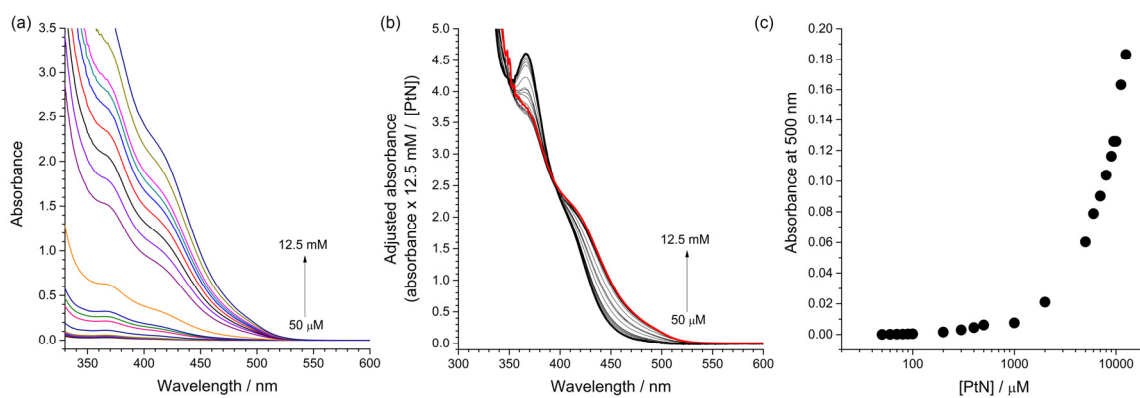


Fig. S8  $^{13}\text{C}\{^1\text{H}\}$  NMR (126 MHz,  $\text{CD}_2\text{Cl}_2$ ) spectrum of (S)-PtBox.



**Fig. S9** Supramolecular assembly formation of PtN.  $^1\text{H}$  NMR (300 MHz,  $\text{CD}_2\text{Cl}_2$ ) spectra obtained for increased concentrations (1, 5 and 10 mM) of PtN in the absence (a) and presence (b) of 1 mM (*R*)-PtBox. The colored vertical bars correspond to the chemical shifts of the aromatic peaks of PtN. The colored asterisk indicates the peak in the PtN assemblies which is shifted from the peak marked with vertical bars in the identical color. The  $^1\text{H}$  NMR spectrum of 1 mM (*R*)-PtBox is included in (b) for comparison. The double blue asterisks in the bottom spectrum in (b) (i.e., 1 mM PtN + 1 mM (*R*)-PtBox) represent the peaks of (*R*)-PtBox. Note that these peaks were affected by the presence of increased concentrations of PtN.



**Fig. S10** Emergence of the metal–metal-to-ligand charge-transfer (MMLCT) transition during the self-assembly of PtN. (a) UV–vis absorption spectra obtained with increased concentrations (50  $\mu\text{M}$ –12.5 mM) of PtN (1,4-dioxane). (b) Adjusted UV–vis absorption spectra. Adjusted absorbance was calculated using the relationship absorbance  $\times$  12.5 mM / [PtN], where [PtN] is the molar concentration of PtN. (c) A plot of the absorbance at 500 nm as a function of [PtN]. Although a full sigmoidal dependence cannot be obtained due to significant scattering at concentrations  $>$  10 mM, the result indicates a dissociation constant ( $K_d$ ) to be greater than 10 mM. This  $K_d$  value corresponds to an association constant  $K_a$  ( $K_a = 1/K_d$ )  $<$  100  $\text{M}^{-1}$ .

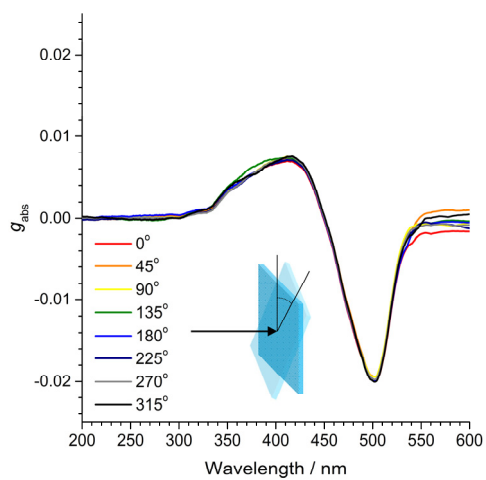


**Fig. S11** Minimal contribution of linear dichroism and birefringence. ECD spectra of the co-assemblies of (S)-PtBox/PtN (2:5, w/w on a quartz substrate) recorded with rotating the substrate (0, 45, 90, 135, 180, 225, 270, and 315°). The invariance of the ECD spectra indicates minimal contribution of linear dichroism and birefringence.



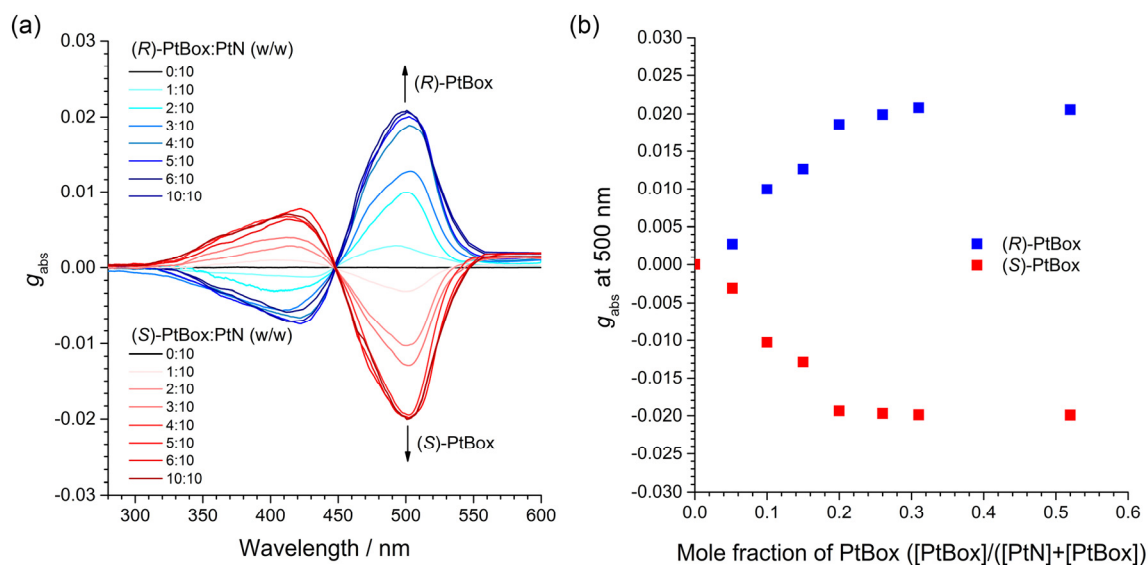


**Fig. S12** Chiral amplification within the co-assemblies of PtBox/PtN. (a) ECD spectra of the co-assemblies of PtBox/PtN obtained with increased concentrations of (*R*)-PtBox (bluish lines) or (*S*)-PtBox (reddish lines). The co-assemblies were prepared by dropcasting 1,2-dichloroethane solutions (2.0 wt % total solute) containing varied ratios of PtBox and PtN (0–10:10, w/w). The black arrows indicate the direction of the spectral changes. (b) Graph depicting  $g_{\text{abs}}$  at 500 nm as a function of the mole fraction of added PtBox. Blue and red points are of (*R*)-PtBox and (*S*)-PtBox, respectively. The  $g_{\text{abs}}$  reach plateaus after the mole fraction of PtBox greater than 0.2, indicating chiral amplification. It is estimated from this result that *ca.* four ( $= [1/0.2] - 1$ ) soldiers follow one sergeant.

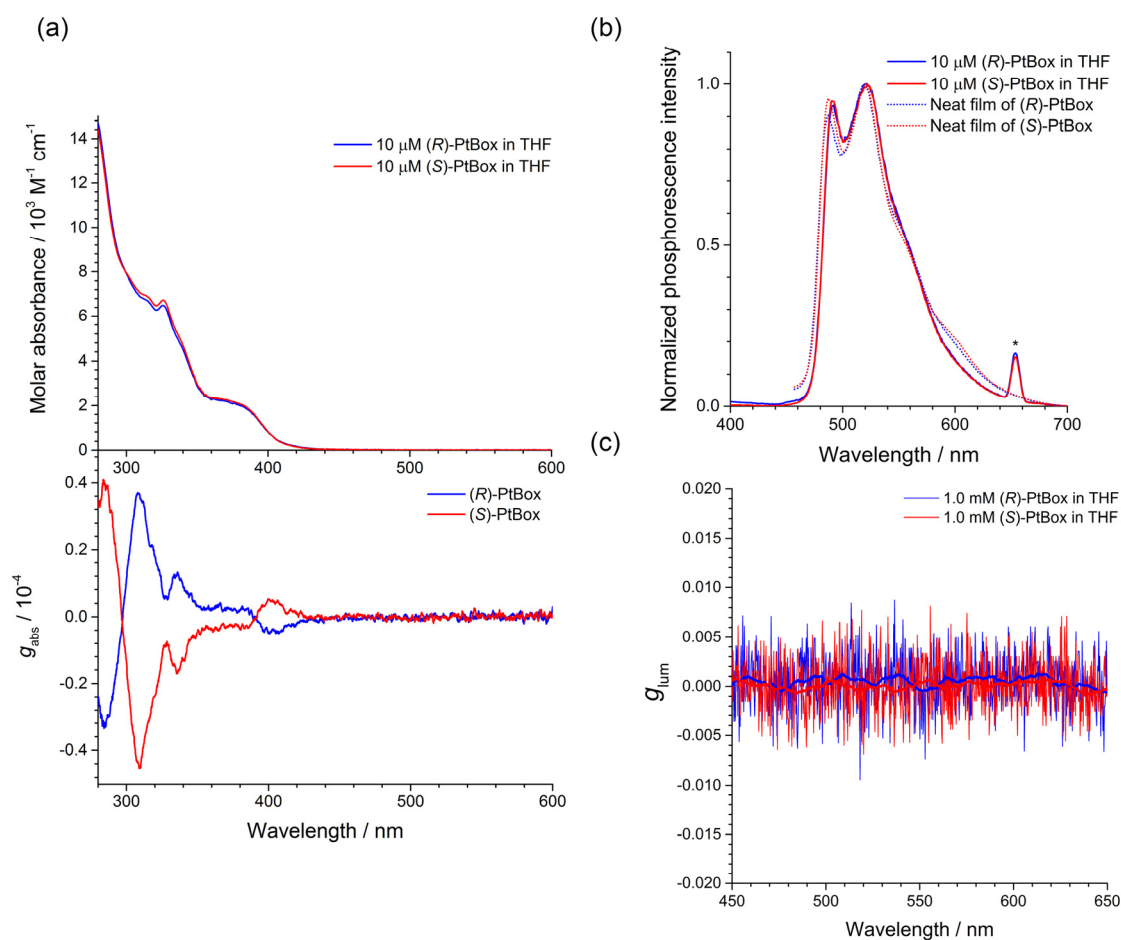


**Fig. S13** Photophysical behaviors of (R)-PtBox (blue) and (S)-PtBox (red). (a) UV-vis absorption (top; 10  $\mu\text{M}$  solutions in THF) and ECD (bottom; 1.0 mM solutions in THF) spectra. (b) Normalized phosphorescence spectra ( $\lambda_{\text{ex}} = 326 \text{ nm}$ ) of the solutions (solid lines; 10  $\mu\text{M}$  solutions in Ar-saturated THF) and neat films (dotted lines) of (R)- and (S)-PtBox. The spectra of the neat films were truncated at wavelengths < 460 nm, due to significant background noises. Peaks marked with an asterisk (\*) are the second harmonic of the excitation beam. (c) Circularly polarized luminescence dissymmetry spectra for Ar-saturated THF solutions (1.0 mM) of (R)- (blue) or (S)-PtBox (red). The CPL measurements were repeated 50 times for each fresh sample, and the average values are plotted. The thick blue and red curves are smoothed spectra of the original data.

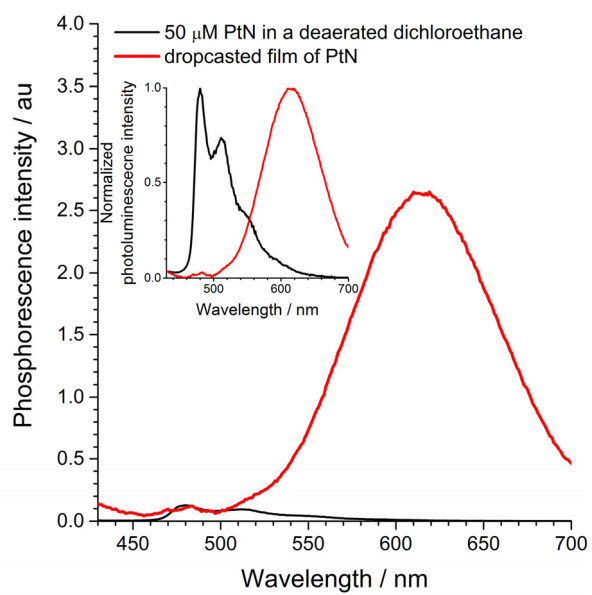


**Fig. S14** Metal–metal-to-ligand charge-transfer phosphorescence. Comparison of the phosphorescence spectra of a deaerated 1,2-dichloroethane solution of 10 μM PtN (black) and a dropcast film (quartz substrate) of PtN (red).  $\lambda_{\text{ex}} = 370$  nm.

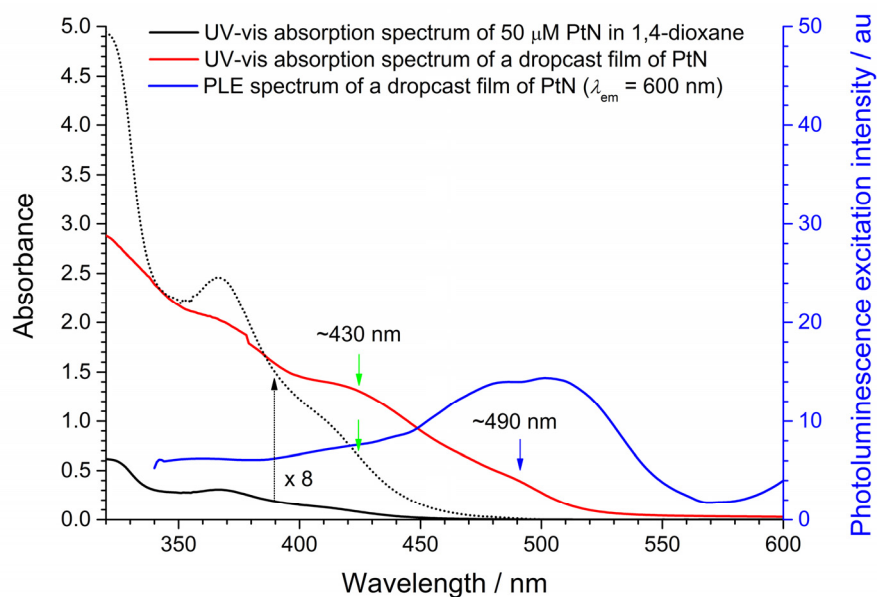


**Fig. S15** Spectral assignment. Spectral identification of the metal-to-ligand charge-transfer (MLCT) and the metal–metal-to-ligand charge-transfer (MMLCT) transitions in PtN assemblies: black, UV–vis absorption spectrum for 50 μM PtN (1,4-dioxane); red, UV–vis absorption spectrum for a dropcast film of PtN (quartz substrate); blue, photoluminescence excitation spectrum (PLE;  $\lambda_{em} = 600$  nm) for the dropcast film of PtN. The green and blue arrows indicate the MLCT and MMLCT transitions, respectively.

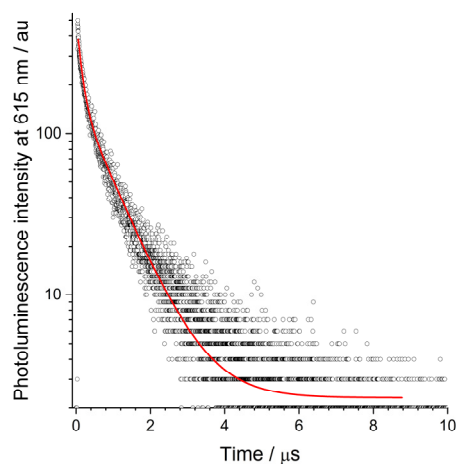


**Fig. S16** Phosphorescence emission of PtN assemblies. Photoluminescence decay traces for the self-assemblies of PtN on a quartz substrate ( $\lambda_{\text{obs}} = 615 \text{ nm}$ ) acquired after pulsed laser photoexcitation at 377 nm. The red curve corresponds to a fit to a biexponential decay model. The fit result is piled in Table S2.

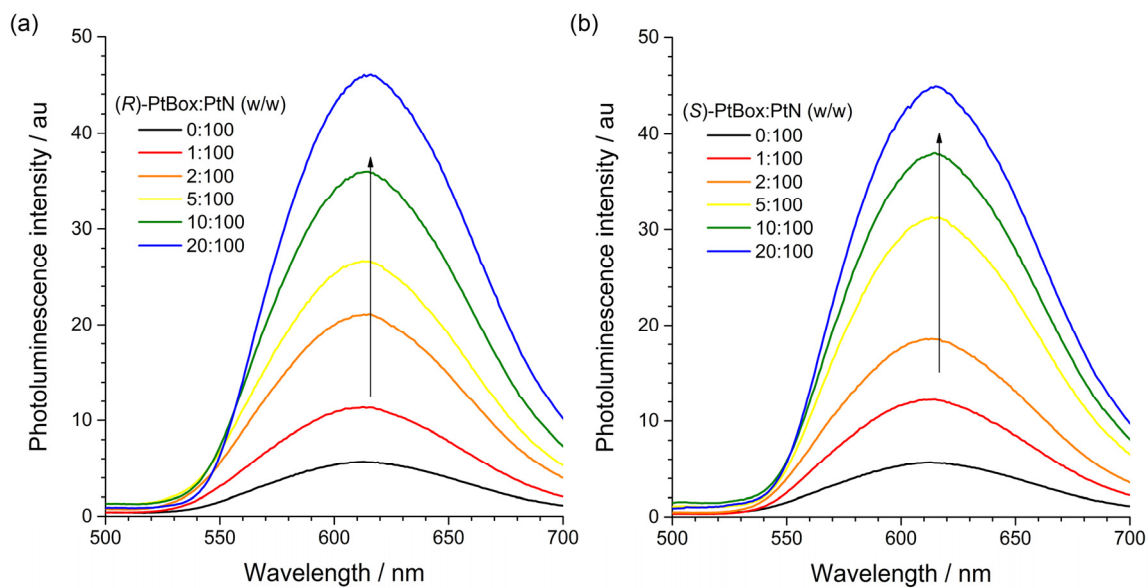


**Fig. S17** Intra-assembly energy transfer from PtBox to PtN. Phosphorescence spectra of the co-assemblies of (R)-PtBox/PtN (a) and (S)-PtBox/PtN (b) obtained under photoexcitation at a wavelength  $\lambda_{\text{ex}} = 363$  nm. The amount of PtN (an energy acceptor) in the PtBox/PtN co-assemblies was fixed, while those of (R)- and (S)-PtBox (energy donors) were increased from 0:100 to 20:100 (PtBox:PtN, w/w). The arrows indicate the direction of the spectral changes.

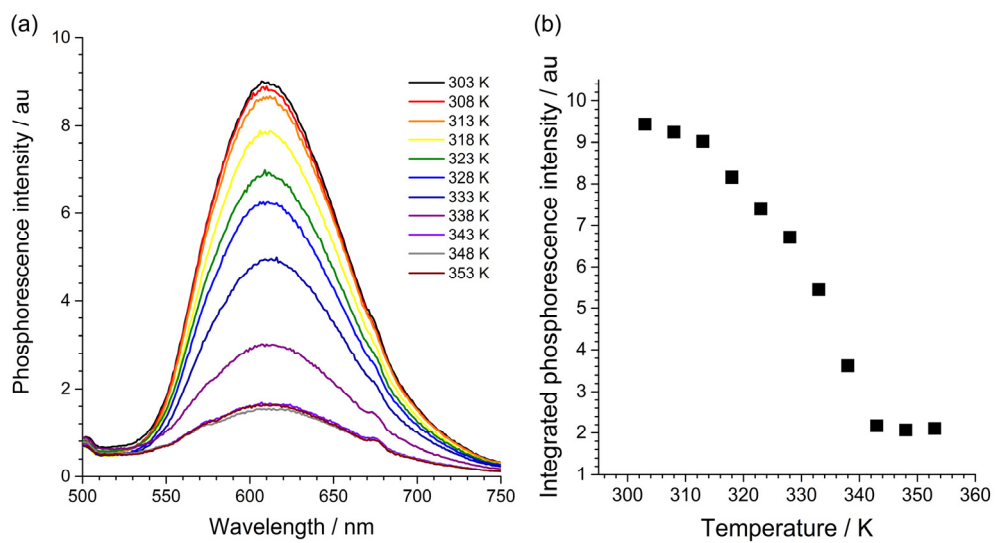


**Fig. S18** Thermal disassembly of the self-assembled PtN. (a) Changes in the phosphorescence spectra of the self-assemblies of PtN upon increasing the temperature (303–353 K). (b) Corresponding changes in the integrated phosphorescence spectra ( $\lambda_{em} = 500\text{--}750\text{ nm}$ ).

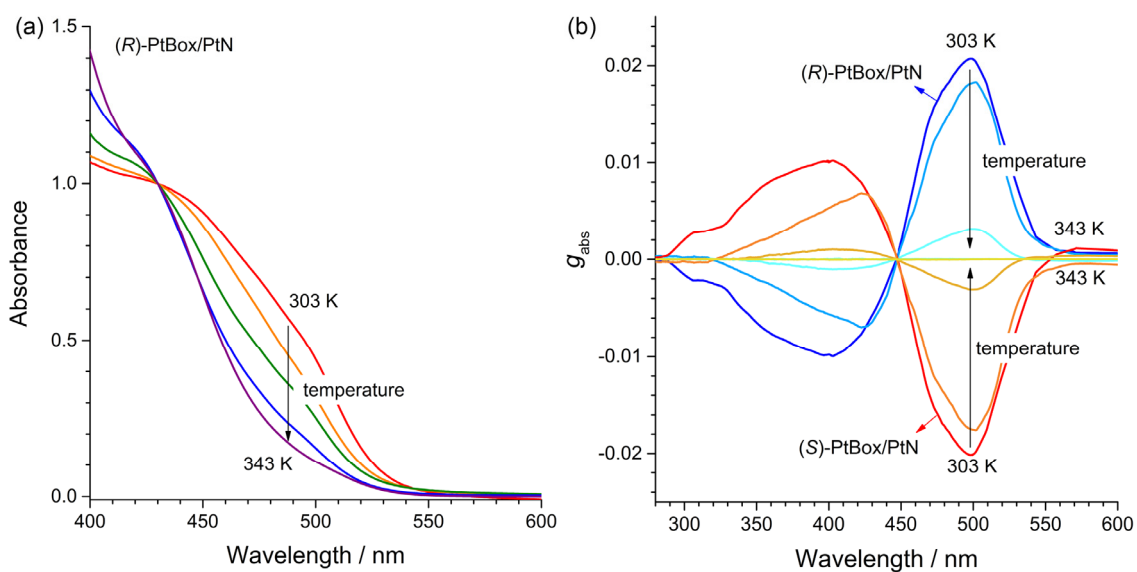


**Fig. S19** Thermal disassembly of the co-assemblies of PtBox/PtN. (a) Changes in the UV-vis absorption spectra of the (R)-PtBox/PtN (2:5, w/w) co-assemblies upon increasing the temperature (303–343 K). (b) Changes in the ECD spectra of the co-assemblies of (R)-PtBox/PtN (2:5, w/w; bluish curves) and (S)-PtBox/PtN (2:5, w/w; reddish curves) upon increasing the temperature (303–343 K).



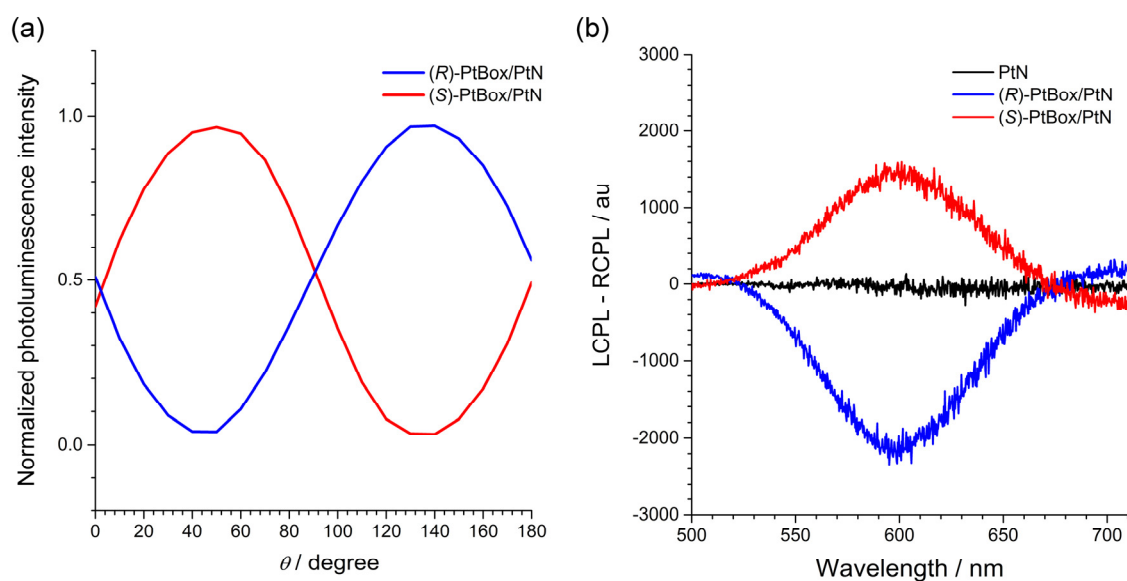


**Fig. S20** Circularly polarized phosphorescence from the co-assemblies of PtBox/PtN. (a) Normalized photoluminescence intensities of the co-assemblies of (R)-PtBox/PtN (blue) or (S)-PtBox/PtN (red) recorded with rotating a quarter-wave retarder.  $\theta$  is a relative angle between the polarization axis of a linear polarizer and the crystal axis of a quarter-wave retarder. (b) The difference spectra of left- (LCPL) and right-handed circularly polarized luminescence (RCPL) of the self-assemblies of PtN (black) and the co-assemblies of (R)-PtBox/PtN (blue) or (S)-PtBox/PtN (red).  $\lambda_{ex} = 365$  nm.

## References

1. M. J. Frisch, G. W. Trucks, H. B. Schlegel, G. E. Scuseria, M. A. Robb, J. R. Cheeseman, G. Scalmani, V. Barone, B. Mennucci, G. A. Petersson, H. Nakatsuji, M. Caricato, X. Li, H. P. Hratchian, A. F. Izmaylov, J. Bloino, G. Zheng, J. L. Sonnenberg, M. Hada, M. Ehara, K. Toyota, R. Fukuda, J. Hasegawa, M. Ishida, T. Nakajima, Y. Honda, O. Kitao, H. Nakai, T. Vreven, J. J. A. Montgomery, J. E. Peralta, F. Ogliaro, M. Bearpark, J. J. Heyd, E. Brothers, K. N. Kudin, V. N. Staroverov, T. Keith, R. Kobayashi, J. Normand, K. Raghavachari, A. Rendell, J. C. Burant, S. S. Iyengar, J. Tomasi, M. Cossi, N. Rega, J. M. Millam, M. Klene, J. E. Knox, J. B. Cross, V. Bakken, C. Adamo, J. Jaramillo, R. Gomperts, R. E. Stratmann, O. Yazyev, A. J. Austin, R. Cammi, C. Pomelli, J. W. Ochterski, R. L. Martin, K. Morokuma, V. G. Zakrzewski, G. A. Voth, P. Salvador, J. J. Dannenberg, S. Dapprich, A. D. Daniels, O. Farkas, J. B. Foresman, J. V. Ortiz, J. Cioslowski and D. J. Fox, *Journal*, 2009.
2. G. Heinrich, S. Schoof and H. Gusten, *J. Photochem.*, 1974, **3**, 315-320.
3. R. Carr, N. H. Evans and D. Parker, *Chem. Soc. Rev.*, 2012, **41**, 7673-7686.
4. Y. Yamamoto, H. Sakai, J. Yuasa, Y. Araki, T. Wada, T. Sakanoue, T. Takenobu, T. Kawai and T. Hasobe, *J. Phys. Chem. C*, 2016, **120**, 7421-7427.
5. C. Shen, E. Anger, M. Srebro, N. Vanthuyne, K. K. Deol, T. D. Jefferson, G. Muller, J. A. G. Williams, L. Toupet, C. Roussel, J. Autschbach, R. Réau and J. Crassous, *Chem. Sci.*, 2014, **5**, 1915-1927.
6. H. Sakai, T. Kubota, J. Yuasa, Y. Araki, T. Sakanoue, T. Takenobu, T. Wada, T. Kawai and T. Hasobe, *J. Phys. Chem. C*, 2016, **120**, 7860-7869.
7. M. Li, S.-H. Li, D. Zhang, M. Cai, L. Duan, M.-K. Fung and C.-F. Chen, *Angew. Chem., Int. Ed.*, 2018, **57**, 2889-2893.
8. T. Kawai, K. Kawamura, H. Tsumatori, M. Ishikawa, M. Naito, M. Fujiki and T. Nakashima, *ChemPhysChem*, 2007, **8**, 1465-1468.
9. E. M. Sanchez-Carnerero, F. Moreno, B. L. Maroto, A. R. Agarrabeitia, M. J. Ortiz, B. G. Vo, G. Muller and S. de la Moya, *J. Am. Chem. Soc.*, 2014, **136**, 3346-3349.
10. S. Feuillastre, M. Pauton, L. Gao, A. Desmarchelier, A. J. Riives, D. Prim, D. Tondelier, B. Geffroy, G. Muller, G. Clavier and G. Pieters, *J. Am. Chem. Soc.*, 2016, **138**, 3990-3993.
11. H. Maeda, Y. Bando, K. Shimomura, I. Yamada, M. Naito, K. Nobusawa, H. Tsumatori and T. Kawai, *J. Am. Chem. Soc.*, 2011, **133**, 9266-9269.
12. T. Imagawa, S. Hirata, K. Totani, T. Watanabe and M. Vacha, *Chem. Commun.*, 2015, **51**, 13268-13271.

13. C. Schaffner-Hamann, A. von Zelewsky, A. Barbieri, F. Barigelletti, G. Muller, J. P. Riehl and A. Neels, *J. Am. Chem. Soc.*, 2004, **126**, 9339-9348.
14. H. Sakai, T. Kubota, J. Yuasa, Y. Araki, T. Sakanoue, T. Takenobu, T. Wada, T. Kawai and T. Hasobe, *Org. Biomol. Chem.*, 2016, **14**, 6738-6743.
15. T. R. Schulte, J. J. Holstein, L. Krause, R. Michel, D. Stalke, E. Sakuda, K. Umakoshi, G. Longhi, S. Abbate and G. H. Clever, *J. Am. Chem. Soc.*, 2017, **139**, 6863-6866.
16. D.-Q. He, H.-Y. Lu, M. Li and C.-F. Chen, *Chem. Commun.*, 2017, **53**, 6093-6096.
17. R. B. Alnoman, S. Rihn, D. C. O'Connor, F. A. Black, B. Costello, P. G. Waddell, W. Clegg, R. D. Peacock, W. Herrebout, J. G. Knight and M. J. Hall, *Chem. Eur. J.*, 2016, **22**, 93-96.
18. T. Otani, A. Tsuyuki, T. Iwachi, S. Someya, K. Tateno, H. Kawai, T. Saito, K. S. Kanyiva and T. Shibata, *Angew. Chem., Int. Ed.*, 2017, **56**, 3906-3910.
19. Y. Morisaki, M. Gon, T. Sasamori, N. Tokitoh and Y. Chujo, *J. Am. Chem. Soc.*, 2014, **136**, 3350-3353.
20. Z. Shen, T. Wang, L. Shi, Z. Tang and M. Liu, *Chem. Sci.*, 2015, **6**, 4267-4272.
21. R. Aoki, R. Toyoda, J. F. Kogel, R. Sakamoto, J. Kumar, Y. Kitagawa, K. Harano, T. Kawai and H. Nishihara, *J. Am. Chem. Soc.*, 2017, **139**, 16024-16027.
22. J. F. Kogel, S. Kusaka, R. Sakamoto, T. Iwashima, M. Tsuchiya, R. Toyoda, R. Matsuoka, T. Tsukamoto, J. Yuasa, Y. Kitagawa, T. Kawai and H. Nishihara, *Angew. Chem., Int. Ed.*, 2016, **55**, 1377-1381.
23. A. Gossauer, F. Fehr, F. Nydegger and H. Stöckli-Evans, *J. Am. Chem. Soc.*, 1997, **1997**, 1599-1608.
24. J. Liu, H. Su, L. Meng, Y. Zhao, C. Deng, J. C. Y. Ng, P. Lu, M. Faisal, J. W. Y. Lam, X. Huang, H. Wu, K. S. Wong and B. Z. Tang, *Chem. Sci.*, 2012, **3**, 2737-2747.
25. Y. Wang, X. Li, F. Li, W.-Y. Sun, C. Zhu and Y. Cheng, *Chem. Commun.*, 2017, **53**, 7505-7508.
26. T. Ikeda, M. Takayama, J. Kumar, T. Kawai and T. Haino, *Dalton Trans.*, 2015, **44**, 13156-13162.
27. H. Qu, Y. Wang, Z. Li, X. Wang, H. Fang, Z. Tian and X. Cao, *J. Am. Chem. Soc.*, 2017, **139**, 18142-18145.
28. A. Satrijo, S. C. J. Meskers and T. M. Swager, *J. Am. Chem. Soc.*, 2006, **128**, 9030-9031.
29. H. Nishimura, K. Tanaka, Y. Morisaki, Y. Chujo, A. Wakamiya and Y. Murata, *J. Org. Chem.*, 2017, **82**, 5242-5249.
30. K. Takase, K. Noguchi and K. Nakano, *Org. Lett.*, 2017, **19**, 5082-5085.

31. C. M. Cruz, I. R. Márquez, I. F. A. Mariz, V. Blanco, C. Sánchez-Sánchez, J. M. Sobrado, J. A. Martín-Gago, J. M. Cuerva, E. Maçôs and A. G. Campaña, *Chem. Sci.*, 2018, **9**, 3917-3924.
32. K. Takaishi, M. Yasui and T. Ema, *J. Am. Chem. Soc.*, 2018, **140**, 5334-5338.
33. N. Hellou, M. Srebro-Hooper, L. Favereau, F. Zinna, E. Caytan, L. Toupet, V. Dorcet, M. Jean, N. Vanthuyne, J. A. G. Williams, L. Di Bari, J. Autschbach and J. Crassous, *Angew. Chem., Int. Ed.*, 2017, **56**, 8236-8239.
34. S. Zhang, Y. Wang, F. Meng, C. Dai, Y. Cheng and C. Zhu, *Chem. Commun.*, 2015, **51**, 9014-9017.
35. S. Koga, S. Ueki, M. Shimada, R. Ishii, Y. Kurihara, Y. Yamanoi, J. Yuasa, T. Kawai, T.-a. Uchida, M. Iwamura, K. Nozaki and H. Nishihara, *J. Org. Chem.*, 2017, **82**, 6108-6117.
36. M. Shimada, Y. Yamanoi, T. Ohto, S.-T. Pham, R. Yamada, H. Tada, K. Omoto, S. Tashiro, M. Shionoya, M. Hattori, K. Jimura, S. Hayashi, H. Koike, M. Iwamura, K. Nozaki and H. Nishihara, *J. Am. Chem. Soc.*, 2017, **139**, 11214-11221.
37. P. H. Schippers and H. P. J. M. Dekkers, *J. Am. Chem. Soc.*, 1983, **105**, 145-146.
38. P. H. Schippers, J. P. M. Van der Ploeg and H. P. J. M. Dekkers, *J. Am. Chem. Soc.*, 1983, **105**, 84-89.
39. Y. Kitayama, K. Nakabayashi, T. Wakabayashi, N. Tajima, M. Fujiki and Y. Imai, *RSC Adv.*, 2015, **5**, 410-415.
40. S. Tanaka, K. Sato, K. Ichida, T. Abe, T. Tsubomura, T. Suzuki and K. Shinozaki, *Chem. Asian J.*, 2016, **11**, 265-273.
41. H. L.-K. Fu, C. Po, H. He, S. Y.-L. Leung, K. S. Wong and V. W.-W. Yam, *Chem. Eur. J.*, 2016, **22**, 11826-11836.
42. J. Song, M. Wang, X. Zhou and H. Xiang, *Chem. Eur. J.*, 2018, **24**, 7128-7132.
43. T. Nishikawa, Y. Nagata and M. Suginome, *ACS Macro Lett.*, 2017, **6**, 431-435.
44. K. Nakamura, S. Furumi, M. Takeuchi, T. Shibuya and K. Tanaka, *J. Am. Chem. Soc.*, 2014, **136**, 5555-5558.
45. M. Yuki, N. Tomoki, F. Ryo, N. Shiho, T. Nobuo, K. Mizuki, F. Michiya and I. Yoshitane, *Org. Biomol. Chem.*, 2017, **15**, 4548-4553.
46. S. Sato, A. Yoshii, S. Takahashi, S. Furumi, M. Takeuchi and H. Isobe, *Proc. Natl. Acad. Sci., USA*, 2017, **114**, 13097-13101.
47. T. Kimoto, N. Tajima, M. Fujiki and Y. Imai, *Chem. Asian J.*, 2012, **7**, 2836-2841.
48. T. Kinuta, N. Tajima, M. Fujiki, M. Miyazawa and Y. Imai, *Tetrahedron*, 2012, **68**, 4791-4796.

49. T. Amako, K. Nakabayashi, T. Mori, Y. Inoue, M. Fujiki and Y. Imai, *Chem. Commun.*, 2014, **50**, 12836-12839.
50. Y. Kitayama, T. Amako, N. Suzuki, M. Fujiki and Y. Imai, *Org. Biomol. Chem.*, 2014, **12**, 4342-4346.
51. Y. Inoue, D. Sakamaki, Y. Tsutsui, M. Gon, Y. Chujo and S. Seki, *J. Am. Chem. Soc.*, 2018, **140**, 7152-7158.
52. Y. Sawada, S. Furumi, A. Takai, M. Takeuchi, K. Noguchi and K. Tanaka, *J. Am. Chem. Soc.*, 2012, **134**, 4080-4083.
53. T. Amako, K. Nakabayashi, A. Sudo, M. Fujiki and Y. Imai, *Org. Biomol. Chem.*, 2015, **13**, 2913-2917.
54. H. Sakai, S. Shinto, J. Kumar, Y. Araki, T. Sakanoue, T. Takenobu, T. Wada, T. Kawai and T. Hasobe, *J. Phys. Chem. C*, 2015, **119**, 13937-13947.
55. F. J. Coughlin, M. S. Westrol, K. D. Oyler, N. Byrne, C. Kraml, E. Zysman-Colman, M. S. Lowry and S. Bernhard, *Inorg. Chem.*, 2008, **47**, 2039-2048.